GEOPHYSICAL ASPECTS OF ATMOSPHERIC REFRACTION

Charles G. Purves

Naval Research Laboratory
Washington, D. C.

7 June 1974

SECURITY CLASSIFICATION OF THIS PAGE (When Data Entered)

REPORT DOCUMENTATION PAGE		READ INSTRUCTIONS BEFORE COMPLETING FORM
1. REPORT NUMBER NRL Report 7725	2. GOVT ACCESSION NO.	3. RECIPIENT'S CATALOG NUMBER AD 780 433
4. TITLE (and Subtitle) GEOPHYSICAL ASPECTS OF ATMOSPHERIC REFRACTION		5. TYPE OF REPORT & PERIOD COVERED Final report on one phase of a continuing NRL Problem. 6. PERFORMING ORG. REPORT NUMBER
7. AUTHOR(s) Charles G. Purves		8. CONTRACT OR GRANT NUMBER(s)
9. PERFORMING ORGANIZATION NAME AND ADDRESS Naval Research Laboratory Washington, D.C. 20375		10. PROGRAM ELEMENT, PROJECT, TASK AREA & WORK UNIT NUMBERS NRL Problem R07-20 RE 12-151-402-4024
11. CONTROLLING OFFICE NAME AND ADDRESS Department of the Navy Office of Naval Research Arlington, Va. 22217		12. REPORT DATE June 7, 1974 13. NUMBER OF PAGES 45
14. MONITORING AGENCY NAME & ADDRESS(if different from Controlling Office)		15. SECURITY CLASS. (of this report) Unclassified 15a. DECLASSIFICATION/DOWNGRADING SCHEDULE

16. DISTRIBUTION STATEMENT (of this Report)

Approved for public release; distribution unlimited.

17. DISTRIBUTION STATEMENT (of the abstract entered in Block 20, if different from Report)

18. SUPPLEMENTARY NOTES

19. KEY WORDS (Continue on reverse side if necessary and identify by block number)

Anomalous radar propagation	Electromagnetic waves	Ray tracing
Cloud correlations	Haze layers	Refractive index forecasts
Cloud mosaic	Microwave refractometer	Refractive index profiles
Convective cloud cells	Radar horizon	Satellite cloud photography
Ducting gradients	Radios	(Continued)

20. ABSTRACT (Continue on reverse side if necessary and identify by block number)

Considerable interest is being generated by the Navy on ways of improving the state of the art in providing better refractive index forecasts (RIF's) needed to upgrade the Navy's capabilities in radar target detection, communication, and other significant propagation effects where atmospheric refraction poses a real concern during naval operations. For a decade during the late 1950's and early 1960's, personnel of the Naval Research Laboratory (NRL) conducted many radar meteorological research flights throughout the world and especially in trade wind regions where anomalous propagation conditions are
(Continued)

19. Keywords (continued)

Temperature inversion
Tiros 3
Experiments I-IV

20. Abstract (continued)

typically associated with a persistent temperature inversion. The intent of this report is to compile many of the significant findings obtained by the NRL research flights so that the geophysical aspects of atmospheric refraction can be viewed from both the theoretical and practical points of view.

From a theoretical point of view a review of the literature is included to provide a general background covering such aspects as the wavelength dependence of atmospheric ducts, the accepted equation for refractive index of air in terms of meteorological parameters, refraction and reflection at a surface of discontinuity, ray path curvature relative to the surface of earth, and the accepted Navy system for classifying refractive index gradients.

From a practical point of view a significant departure from the standard atlas concept, which uses radiosonde data, is presented to show worldwide oceanic regions of persistent atmospheric duct layers. Examples of anomalous propagation in the form of radar scope pictures, cloud diagrams, ray tracing, and radar signal-strength measurements that are typically associated with elevated duct layers that extend normal radar ranges hundreds of miles beyond the radar horizon are shown. Significant correlations that link temperature inversion magnitude with cloud type and the extent of continuous duct layers with cloud and haze layers are shown. The use of satellite cloud photography for making propagation forecasts is discussed. The state of the art in making a RIF is discussed, and recommendations on improving the Navy's present radar forecasting capabilities are made.

CONTENTS

GEOPHYSICAL ASPECTS OF ATMOSPHERIC REFRACTION

INTRODUCTION

Today's Navy has an increasing demand to gain a better understanding of anomalous propagation effects on operational radars. The need exists to develop operational refractive index forecasts (RIF's) that can be used by the fleet. The state of the art in providing reliable RIF's seriously lags the development of highly sophisticated radars. In the Spring of 1972 the Joint Chiefs of Staff took action with its Interservice Committee on Meteorological Products and Services to appoint a triservice working group to discuss and take action on the need for RIF's. This committee met on May 22 and 23, 1972, and initiated a triservice Joint Refractive Radio/Radar Index Forecast Working Group. More recently, in May 1973, the Navy sponsored a 3-day conference on *Refractive Effects on Electromagnetic Propagation* in San Diego. This conference was well attended by many key naval, military and civilian, operational and scientific, personnel. Subjects reviewed were the current state of the art in obtaining RIF's; fleet requirements concerning the educational, research and development, and operational efforts needed to improve the Navy's capabilities in radar target detection; communication; and other significant anomalous propagation effects where atmospheric refraction poses a real concern during naval combat operations. As can be seen, considerable interest by the Navy, and the other military services, is being generated at this time to bring to light the military significance that anomalous atmospheric propagation has on radars.

The purpose of this paper is to discuss some of the geophysical aspects of atmospheric refraction and its effect on radars. Of special concern will be the cause-and-effect relationships associated with the trapping of electromagnetic energy into atmospheric duct layers that result in anomalous propagation conditions and extend radar ranges far beyond the normal radar horizon.

WAVELENGTH DEPENDENCE OF DUCTS

As early as 1948, Dr. H. G. Booker [1], an English scientist, gave an indication that there was a wavelength dependence for trapping radio energy into an elevated duct layer. However, no general equations were given at that time to show a mathematical relationship. In general, Dr. Booker's observation was that the greater the wavelength, the greater the depth of the duct layer for trapping. In 1954, a U.S. Navy meteorological publication [2] contained a table, consisting of four entries, that gave the maximum wavelength as a function of duct height, but again no general equation was given to satisfy the entries in the table (Table 1 of this report).

Note: Manuscript submitted January 29, 1974.

Table 1
Maximum Duct Thicknesses Required to Trap Radiation
From Specific Wavelength Radars

Wavelength λ(cm)	Maximum Duct Thickness, d	
	(ft)	(cm)
1	16	488
10	80	2,438
100	400	12,192
1,000	2,000	60,960

In 1965 a standard radar textbook [3] included the following equation for the same set of values published in the 1954 Navy publication:

$$\lambda = 0.014d^{3/2} \tag{1a}$$

where λ = wavelength and d = maximum duct thickness for trapping. In this equation the units are mixed (i.e., λ is in centimeters and d is in feet. Converting Eq. (1a) to an equation in which both λ and d are in centimeters yields:

$$\lambda = 8.31966d^{1.5} \times 10^{-5} . \tag{1b}$$

However, a mathematical check on Eq. (1b) using the values given Table 1 indicates discrepancies on the order of 20%. A better mathematical expression with λ in centimeters and d in feet would be

$$\lambda = \left(\frac{d}{16}\right)^{1.43068} . \tag{2a}$$

The conversion of Eq. (2a) to an equation in which both λ and d are in centimeters yields

$$\lambda = 5.67147(1.905d)^{1.43068} \times 10^{-5} . \tag{2b}$$

The intended use of the equation was to obtain the maximum duct thickness for trapping for radars of known wavelengths. Consequently, Eq. (3a) is valid if d is in feet and λ is in centimeters, and Eq. (3b) is valid when both d and λ are in centimeters:

$$d = 16\lambda^{0.69897} \tag{3a}$$

and

$$d = 482.88\lambda^{0.69897} . \tag{3b}$$

Table 1 satisfies the conditions of Eqs. (3). As can be seen from the values in Table 1, wavelengths greater than 1000 cm (10 m) would require extremely large duct thicknesses

to trap electromagnetic energy into a duct layer. Because duct thicknesses of 2000 ft seldom occur in the atmosphere, radars having wavelengths greater than 10 m are quite unaffected or impervious to trapping by a ducting layer. For this reason elevated duct layers less than 2000 ft would be capable of trapping electromagnetic energy only from radars whose wavelengths are less than 10 m.

Because there are more operational radars with wavelengths below 1 m, most of the critical duct thicknesses for trapping energy into an elevated duct layer would be less than 400 ft. Shallow surface and elevated duct layers whose thicknesses are less than 80 ft would only be trapped by radars whose wavelengths are less than 10 cm.

A more meaningful interpretation of the Table 1 values would be to show the critical ducting parameters of wavelength and duct thicknesses for trapping as related to specific radar frequency bandwidths as defined in standard radar textbooks [4]. This is readily done by use of the general equation relating speed of propagation v to wavelength λ and frequency f:

$$v = \lambda f . \tag{4}$$

By using Eqs. (3) in conjunction with Eq. (4), it is possible to obtain the critical ducting and radar parameters related to the various radar bands presented in Table 2.

Table 2
Critical Ducting Parameters as a Function of Radar Frequency Bands

Radar Frequency Band	Frequency Range (MHz)	Wavelength Range (cm)	Maximum Duct Thickness d	
			(ft)	(m)
VHF	30 to 300	1000 to 100	2000 to 400	609.6 to 121.9
UHF	300 to 1000	100 to 30	400 to 172	121.9 to 52.4
L	1000 to 2000	30 to 15	172 to 106	52.4 to 32.3
S	2000 to 4000	15 to 7.5	106 to 65	32.3 to 19.8
C	4000 to 8000	7.5 to 3.75	65 to 40	19.8 to 12.2
X	8000 to 12 500	3.75 to 2.4	40 to 30	12.2 to 9.1
K	12,500 to 40,000	2.4 to 0.75	30 to 13	9.1 to 4.0

THE RELATIONSHIP OF VELOCITY AND REFRACTIVE INDEX

In the study of the propagation of electromagnetic waves through earth's atmosphere it can be shown that the speed of propagation is directly related to the refractive index of air and that the bending, or refraction, is related to the gradient of the refractive index. It is necessary to have a basic concept of these relationships before attempting to depict the point-to-point trajectory, or ray path, that occurs in the propagation of electromagnetic energy.

Experiments have proven that both optical light and electromagnetic waves when transmitted through a homogeneous medium, such as air, travel at identical speeds. The following velocity equation is generally accepted as representative for the case of electromagnetic waves:

$$v = \frac{c}{\sqrt{\mu k}} \tag{4}$$

where

c = the velocity
μ = the magnetic permeability
k = the dielectric constant of the medium.

For all practical purposes, the value of the magnetic permeability μ may be taken as unity, and by accepted definition the following relationship exists for the refractive index n and k:

$$n = \sqrt{k}. \tag{6}$$

Consequently Eq. (5) may be rewritten as

$$v = \frac{c}{n}. \tag{7}$$

It is this relationship that links radar frequency and wavelength parameters with critical duct thicknesses and refraction anomalies.

Under normal atmospheric conditions, both the refractive index and air density values increase when going from higher to lower altitudes or when passing from drier to more moist air. Any increase in the value of the refractive index of air will result in a slightly slower speed in the velocity of electromagnetic waves. For example, in free space where vacuum conditions exist, $n = 1.0000$ and $v = 299{,}793.0$ km/s. At sea level the maximum expected refractive index value would not exceed 1.0004. Using this value for n would give a corresponding velocity v of 299,673.1 km/s. Consequently, the maximum change in the propagation of electromagnetic waves between free space and sea level is about 120 km/s. For certain radar systems, such as in aerial electronic-surveying and space-tracking radars, significant velocity changes occur and must be taken into consideration.

REFRACTION AND REFLECTION AT A SURFACE OF DISCONTINUITY

By defining a surface of discontinuity as a surface, or boundary level, at which there is a significant change in atmospheric density, it is possible to show that there is a definite relationship between the speed of propagation and the amount of refraction that occurs when passing from one density level to the next. Figure 1 illustrates how an incident ray is refracted or reflected at a surface of discontinuity. Refraction and

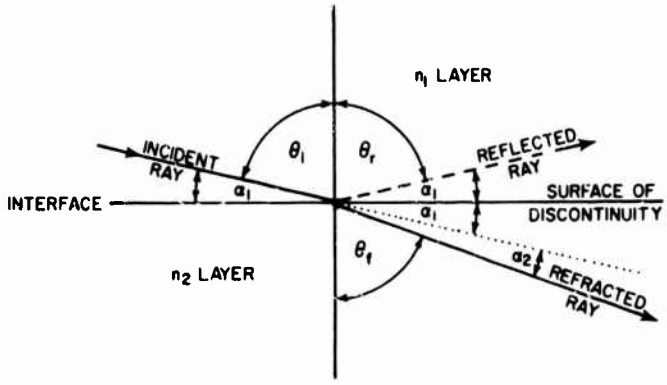

Fig. 1—Bending characteristics at a surface of discontinuity

reflection of the incident ray, shown in the figure depicted by the solid and dashed arrow lines, follow the principles of Snell's Law [5] for refraction,

$$\frac{\sin \theta_i}{\sin \theta_f} = \frac{n_2}{n_1}, \tag{8}$$

where

n_1 = refractive index value of the n_1 layer
n_2 = refractive index value of the n_2 layer
θ_i = the angle of incidence for layer n_1
θ_r = the angle of reflection for layer n_1
α_1 = $90^\circ - \theta_i$ = complementary angle to θ_i (or grazing angle)
$2\alpha_1$ = angular deflection of the scattered ray with respect to the incident ray,
α_2 = angular deflection of the refracted ray with respect to the incident ray, and
θ_f = the angle of refraction for layer n_2.

From Eq. (8) it is apparent that $\theta_f < \theta_i$ when $n_2 > n_1$. From Fig. 1 it is seen that $\theta_i = \theta_r$.

The general interface problem requires a scattered ray as well as a refracted ray. It is well known that the relative intensities of the scattered and refracted rays depend on the angle of incidence θ_i and the ratio of the refractive index of each layer n_1/n_2. The trapping of waves within an atmospheric duct layer involves a specific angle of incidence. Once this angle is attained, critical ducting gradients can cause sufficient bending to refract the energy of the incident ray into the duct layer. In the case of ducting, the critical acceptance angle ϕ_c for refraction into the duct is based on the relationship

$$\phi_c = \sin^{-1} \frac{n_1}{n_2}. \tag{9}$$

For all practical considerations the ratio $n_1/n_2 \approx 1$; therefore, the critical acceptance angle $\phi_c \approx 1°$. In terms of the diagram in Fig. 1, trapping occurs when the grazing angle α_1 is equal to ϕ_c. Therefore the critical incidence angle θ_i to refract the incident ray into the duct is the complement of the critical grazing angle α_1 is 89°. Consequently, only rays launched nearly parallel (within 1°) of the duct interface level, or duct axis, are trapped. Therefore, the amount of refraction, or bending, to get into the duct layer is not very large. Once ducting occurs, the rays will continue to remain in the duct layer as long as a ducting gradient exists between layers n_1 and n_2. After trapping occurs, the principal relationship that keeps the ray path in the n_2 layer where ducting occurs is primarily governed by the laws of reflection.

According to total reflection theory, radiation in a more dense medium (n_2 layer) meeting the boundary of a less dense medium (n_1 layer) at an angle greater than the critical angle will be totally reflected back into the more dense medium where $n_2 > n_1$. For this reason, once the radient energy is refracted into the more dense n_2 layer, the rays are continually contained in the duct layer by reflection at the duct interface as long as a trapping refractive index gradient exists. The principles of total reflection theory help to explain why low-energy output transmitters are capable of transmitting measurable signals via an elevated duct layer for hundred and at times thousands of miles beyond the normal radar horizon ranges with virtually no signal losses.

The speed of electromagnetic wave propagation in layers n_1 and n_2 is

$$v_1 = \frac{c}{n_1} \tag{10}$$

and

$$v_2 = \frac{c}{n_2}. \tag{11}$$

THE REFRACTIVE INDEX EQUATION

The magnitude of the refractive index of air n has a rather small range of from unity, in free space, to approximately 1.0004 at sea level. In radar meteorology it is more convenient to facilitate numerical computations of n as follows:

$$N = (n - 1)10^6 . \tag{12}$$

This version is sometimes referred to as the "refractivity" index; computed values of N are commonly referred to as N units. Values of N units can be numerically computed as a function of standard meteorological parameters where the general equation for N takes the form

$$N = \frac{A}{T}\left(P + \frac{Be}{T}\right) \tag{13}$$

where

T = Kelvin temperature
P = total atmospheric pressure (in millibars)
e = vapor pressure (in millibars).

The values of constants A and B have been investigated many times by scientific experiments. The National Bureau of Standards endorses the statistical evaluation of Smith and Weintraub [6], as published in 1953, where $A = 77.6$ and $B = 4810$. Insertion of these constants into the general equation for N gives

$$N = 77.6\frac{P}{T} + (3.73 \times 10^5)\frac{e}{T^2} \tag{14}$$

where the first term is generally referred to as the "dry" air term and the second term the "moist" or "wet" air term of the refractive index equation.

The refractive index equation N as shown in Eq. (14) has the general mathematical form of a second-degree polynominal equation. To visualize the effect each of the meteorological parameters P, T, and e has on the refractive index equation N, it is necessary to determine their respective partial differential equations. The following set of partial differential equations is presented to show how a unit change in pressure P, temperature T, and vapor pressure e affects the value of N:

$$\frac{\partial N}{\partial P} = \frac{77.6}{T}, \tag{15}$$

$$\frac{\partial N}{\partial T} = \frac{-77.6}{T^2}\left(P + \frac{9613.4e}{T}\right), \tag{16}$$

and

$$\frac{\partial N}{\partial e} = \frac{373\,000}{T^2}. \tag{17}$$

In the above equations it can be seen that all of the partial derivatives have a temperature dependence. The partial derivatives of Eqs. (15) and (17) depend only upon the temperature, whereas in Eq. (16) the partial derivative $\partial N/\partial T$ is a function of all three meteorological parameters P, T, and e. Table 3 is presented to show the respective N unit changes that occur due to a unit change in arbitrarily selected values of pressure, temperature and vapor pressure. The tabular values presented in Table 3 are representative of typical maximum and minimum atmospheric conditions one would expect in regions where ducting normally occurs. Inspection of the partial derivatives obtained for the representative maximum and minimum cases indicates negligible differences of less than 1 N unit. Consequently, the average derivatives can be evaluated to see what significant relationship exists between them. For example, the approximate average value of

Table 3
Expected N Unit Changes for a Unit Change in Selected Values of P, t, and e

Temperature t (°C)	Pressure P (mb)	Vapor Pressure e (mb)	$\frac{\partial N}{\partial P}$	$\frac{\partial N}{\partial T}$	$\frac{\partial N}{\partial e}$
27.0	1013.25 (sea level)	30	0.3	-1.7	4.1
0.0	767.0 (~ 7500-pressure height)	5	.3	-1.0	5.0

$$\frac{\partial N}{P} = 0.3, \quad \frac{\partial N}{\partial T} = -1.35, \quad \frac{\partial N}{\partial e} = 4.55$$

indicate that the vapor pressure derivative $\partial N/\partial e$ is about 15 times greater than the pressure derivative $\partial N/\partial P$ and about 3.4 times greater than the temperature derivative $\partial N/\partial T$. Consequently, it is most important to be able to measure the vapor pressure term e with accuracy, as this is the most significant term affecting the refractive index equation N.

RAY PATH CURVATURE RELATIVE TO THE SURFACE OF EARTH

It is common knowledge that earth's atmosphere causes significant bending, or refraction, of electromagnetic waves propagated in space, especially in the lower levels of the tropopause. Point-by-point analysis of a single electromagnetic ray in space can be a very complicated process to evaluate when the refractive index gradients do not follow predictable, or measurable, behavior laws in nature. Consequently, the best approach is to consider the simplest cases for fixed or assumed conditions and go from there with other assumptions that will lead to the development of the more complicated cases that occur in nature.

The simplest case for explaining the basic geometry of ray bending is that in which no atmosphere exists, hence all rays would be assumed to travel in a straight line. Figure 2, illustrates this case.

In Fig. 2, point R represents a radar antenna at a height H above earth's surface. The distance D represents the distance to the radar horizon. The line RP represents the horizon line and is tangent to earth's surface at point B. The horizon height h at point P is at a distance d beyond the tangent point, and the lines OA, OB, and OC represent the radius of earth where the radius is equal to a. In this model it can be proven that

$$a^2 + D^2 = (a + H)^2 , \tag{18}$$

and therefore

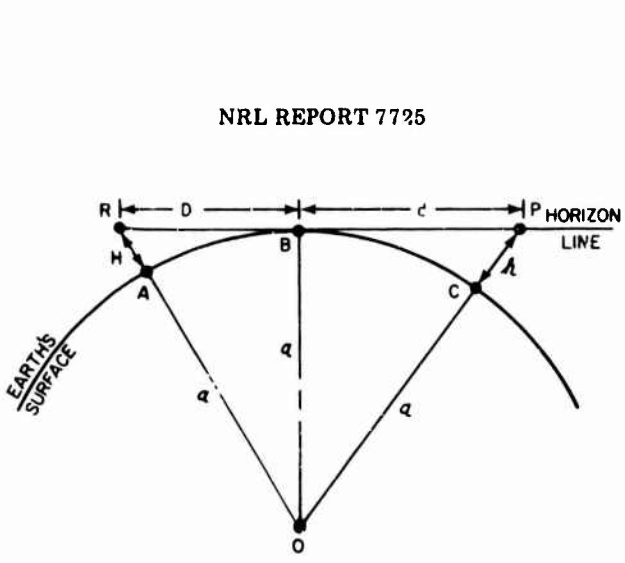

Fig. 2--Ray-path geometry for a spherical earth (case with no atmosphere)

$$D^2 = 2aH + H^2 . \tag{19}$$

Because H is much smaller than $2a$, the second-order term H^2 can be neglected; therefore,

$$D \approx \sqrt{2aH} \tag{20}$$

and

$$H \approx \frac{D^2}{2a} . \tag{21}$$

Similarly, we can also prove that

$$d \approx \sqrt{2ah} \tag{22}$$

and

$$h \approx \frac{d^2}{2a} . \tag{23}$$

It should be noted that the above equations, applicable for the nonatmosphere case, also apply to a homogeneous atmosphere case where no refraction gradients occur.

In the case of a homogeneous atmosphere, where density is constant with altitude, electromagnetic waves travel in straight lines and are not subject to bending. Consequently, the curvature of the rays relative to earth's surface would be $1/a$. Because earth has an atmosphere, the gradient of refraction dn/dH causes bending that differs slightly from the $1/a$ curvature case. In meteorology it is common practice to refer to a standard atmosphere [7], a fictitious atmosphere that closely approximates the average conditions of earth's actual atmosphere. In the standard atmosphere case, the index of refraction n decreases with height at an approximate gradient rate of $-.12N$ units per 1000 ft. The propagation of electromagnetic waves in a standard atmosphere causes bending of rays that are smaller than the $1/a$ case for a homogeneous atmosphere. An acceptable derivation that relates

the curvature of a ray relative to earth's surface for actual atmospheric conditions indicates that the bending relationship adheres to the following equation [8]:

$$\frac{d\phi}{ds} = \frac{1}{R} + \frac{dn}{dh} \tag{24}$$

where

ϕ = the bending angle
s = distance
R = radius of earth, a.

From Eq. (24) it can be shown that in the actual atmosphere where dn/dh decreases with height, a ray path that is concentric, or parallel, to earth's curvature meets the criteria

$$\frac{1}{a} = \frac{-dn}{dh} . \tag{25}$$

Under actual refraction conditions in the atmosphere, trapping (or ducting) conditions occur only when the angle of the ray is within 1° of being parallel to earth's curvature. Rays whose angles are greater than 1° from earth's horizon normally penetrate right through a ducting layer. Consequently, for trapping to occur, both the magnitude of the bending angle ϕ and the refractive index gradient dn/dh must adhere to critical limits. The critical angle ϕ_c has already been defined as being about 1°. Equation (25) also satisfies the conditions for the critical refractive index gradient dn/dh that would cause trapping and cause the ray path to parallel earth's curvature. For convenience, we express earth's curvature in feet, refractive index as N, and the gradient dN/dh in N units per 1000 ft, where

$$dN = N_{h_2} - N_{h_1} \tag{26}$$

and

$$dh = h_2 - h_1 . \tag{27}$$

Standard Mathematical Tables [9] gives the mean radius of earth as 3959 mi. The conversion from miles to feet would give the mean radius of earth as

$$\approx 20.9 \times 10^6 \text{ ft}, \quad \text{or} \quad a \approx 20.9 \times 10^6 \text{ ft}. \tag{28}$$

Because N has been defined as being equal to $(n - 1)10^6$, the conversion of the refractive index gradient in terms of N units becomes

$$\frac{dn}{dh} = \frac{dN}{dh} 10^{-6} . \tag{29}$$

If Eqs. (26) through (29) are used, Eq. (25) can be rewritten as

$$\frac{1}{20.9(10)^6} = -\left(\frac{N_{h_2} - N_{h_1}}{h_2 - h_1}\right) 10^{-6} \tag{30}$$

or

$$\frac{N_{h_2} - N_{h_1}}{h_2 - h_1} = -\frac{1}{20.9} = -0.04785\,. \tag{31}$$

Equation (31) now represents the critical refractive index gradient (dN/dh) for trapping where

$$\left(\frac{dN}{dh}\right) \approx -0.048\,. \tag{32}$$

For convenience, when this gradient is expressed in terms of N units per 1000 ft, we have

$$\left(\frac{dN}{dh}\right) \approx -48N \text{ units per 1000 ft.} \tag{33}$$

Consequently, whenever a negative refractive index gradient of $48N$ units per 1000 ft occurs, trapping can be expected for the rays within 1° of the layer of discontinuity.

A CLASSIFICATION SYSTEM FOR REFRACTION

The gradient change of the index of refraction N under normal atmospheric conditions can be evaluated in both the horizontal and vertical directions. The most persistent and strongest gradients are normally associated with the vertical profiles of N, if one considers the mesoscale or macroscale fields. However, it should be noted that when strong ducting gradients of dN/dh are observed, there may be a flat wavy undulation of the duct layer. Consequently, strong refractive gradients, normally associated with a gradient height relationship, can also be measured in the horizontal field if one takes the microscale field into account.

The Navy has adopted a general classification system [10] of identifying atmospheric refractive index gradients, mainly for forecasting and climatological purposes. The system identifies four separate categories of refractive index gradients:

1. *Subrefraction*—N increases with height. Rays curve upward with reference to a straight line (opposite in direction to the curvature of earth's surface). Radio and radar ranges are significantly reduced; occurrence is quite rare.
2. *Normal*—N decreases with height; the range of dN/dh per 1000 ft is from 0 to 24. Rays curve downward (in the same direction as the curvature of earth's surface) but not as sharply as those in the superrefraction case. Radio and radar performance is generally undisturbed.

3. *Superrefraction*—N decreases with height; the range of dN/dh per 1000 ft is from 24 to 48. Rays curve downward (in the same direction as the curvature of earth's surface) more sharply than those in the normal refraction case but not as sharply as earth's surface. Radio and radar ranges are significantly extended; occurrence is quite frequent.

4. *Trapping*—N decreases with height; the range of dN/dh per 1000 ft is greater than 48. Rays curve downward more sharply than the curvature of earth's surface. Radio and radar performance is greatly disturbed (e.g., ranges are extended greatly and radar holes appear); occurrence is not frequent.

AREAS OF THE WORLD WITH PERSISTENT OCEANIC DUCTING CONDITIONS

The two most significant large-scale meteorological phenomena that cause the trapping of electromagnetic waves into an effective atmospheric waveguide are related to the trade wind temperature inversion and large-scale subsidence. Strong and persistent elevated duct layers over at least one-third of the surface of the oceans are commonly observed throughout the year.

The principal source region of the trade wind inversion is normally on the west coast side of continents, usually close to mountain ranges. Enhancement of the strength of the temperature inversion is related to the downslope gravity winds that heat and dry the air as it flows from the mountains to the seas. Such winds are sometimes locally referred to by such names as Foehn, Santa Ana and Chinook winds. Within several hundred miles of coastal areas such as California, Chile, Southwest Africa, and Angola, where the trade wind inversion originates, the normally elevated duct layers associated with the temperature inversion layer may at times extend to the surface. In all of these principal source regions of the trade wind inversion, the large-scale flow follows the coastline toward the Equator and then flows from the continents in an easterly direction on both sides of the Equator. This easterly trade wind circulation follows the bottom side of large oceanic high-pressure cells in the Northern Hemisphere and the top side of highs in the Southern Hemisphere. The strength of the trade wind inversion weakens in the downstream direction. As it weakens it also rises. Consequently, there normally is a relationship between temperature inversion height and the magnitude of the trade wind inversion.

Large-scale subsidence is associated with high-pressure areas. Large, permanent-high-pressure cells dominate the surfaces of the oceans in both hemispheres between the 15° and 45° latitude belts. In the summer months, in both hemispheres, there is a 5° to 10° poleward shift of these large oceanic high-pressure cells. These cells play a major role in the steerage of global frontal weather storm systems in that they block and deter the penetration of frontal weather, which keeps the major storm tracks to the poleward side of the high. The statistically stable characteristics normally associated with high pressures are those of good weather conditions, generally weak winds and clear skies in the center, and low stratus clouds around the peripheral regions. These characteristics are the result of large-scale subsidence, which produces significant temperature inversions and results in strong ducting gradients to form above the base of the inversion.

Standard worldwide atlas presentations of radio refractivity conditions are generally based on radiosonde measurements of pressure, temperature, and humidity. The slow response time of these instruments masks the full-scale detection of these parameters, which limits the interpretation of refractive index gradients. As a result, the statistical analysis portraying the frequency of occurrences for ducting gradients in the atmosphere contains values that are far too low, perhaps by as much as a factor of 5 to 10. To show appropriate statistics, the observed data must be measured by fast-response instruments whose lag times are on the order of 0.01 s or faster. The microwave refractometer is a fast-response instrument that measures the refractive index of air directly, rather than determining it indirectly through measurements of P, t, and e and allows for reliable measurements of the significant ducting refractive index gradients.

Until adequate statistics are obtained by reliable refractive index measurements over the oceans, any analysis will be biased or subjective and open to criticism. Current world atlas [11] presentations indicate frequencies of occurrence of negative trapping gradients greater than or equal to 48N per 1000 ft for seasonal months of the years, averaging about 5% of the time over such trade wind routes as San Diego to Honolulu or Ascension Island to Recife, Brazil. In contrast to these statistics are the results obtained from the extensive research flights made by NRL over these routes that indicate very high persistent frequencies of occurrence, generally in excess of 50% to 75% of the time. On the basis of at least 100 or more transits over these trade wind routes and the overall correlations of continuous stratus and continuous duct layers, an attempt is made to show where persistent oceanic elevated duct layers are expected. Figures 3a and 3b depict the probability estimates of encountering oceanic ducting layers having negative refractive index gradients greater than or equal to 48N per 1000 ft for the seasonal months of February and August, respectively. The intent of the figures is to consider only the areas that have such gradients more than 30% of the time and to show some indication of the areas where these gradients are even more persistent. The knowledge gained from over 1000 hr of meteorological research flights over the North and South Atlantic, North and South Pacific, Indian Ocean, Red Sea, and Mediterranean Sea during which microwave refractometer, fast-response humidiometer (vapor pressure), fast-response temperature, pressure, cloud diagrams, and radar signal-strength measurements were continuously recorded was incorporated with climatology and satellite cloud photography data to form the basis for the maps in Figs. 3. Figure 3a depicts persistent oceanic atmospheric duct layers for February and is representative of wintertime conditions in the Northern Hemisphere and summer conditions in the Southern Hemisphere. Figure 3b depicts representative conditions for August. Four separate percentage frequency ranges representing the probability estimates of encountering ducting layers having negative refractive index gradients greater than or equal to 48N per 1000 ft are shown in Figs. 3. The frequency ranges are 30% to 45%, 45% to 60%, 60% to 75%, and greater than 75%. For the most part, the 30% to 45% outer boundaries are based on world atlas [12] analysis of sea level pressures using the 1015-mb contour. Consequently, the average pressures contained in the 30% to 45% range depict the areas of large oceanic high-pressure cells that are greater than or equal to 1015 mb. This arbitrary approach is based on the concept that persistent subsidence occurs within the average boundary lines of oceanic high-pressure cells and that a high correlation exists for having persistent temperature inversions and ducting conditions. The main exception to this is in the equatorial regions between Africa and South America where both the experience of many research flights in this area plus the evaluation of cloud satellite

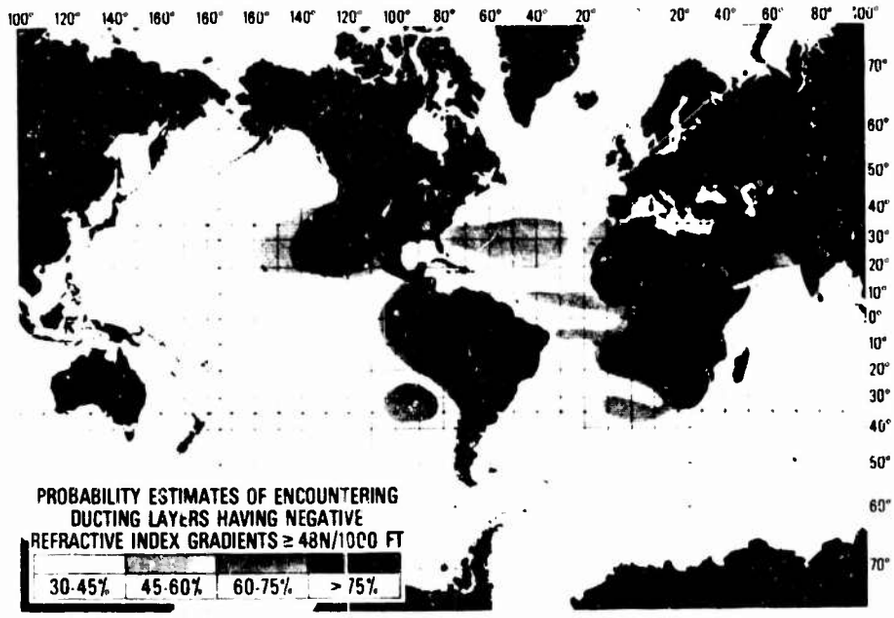

(a) February

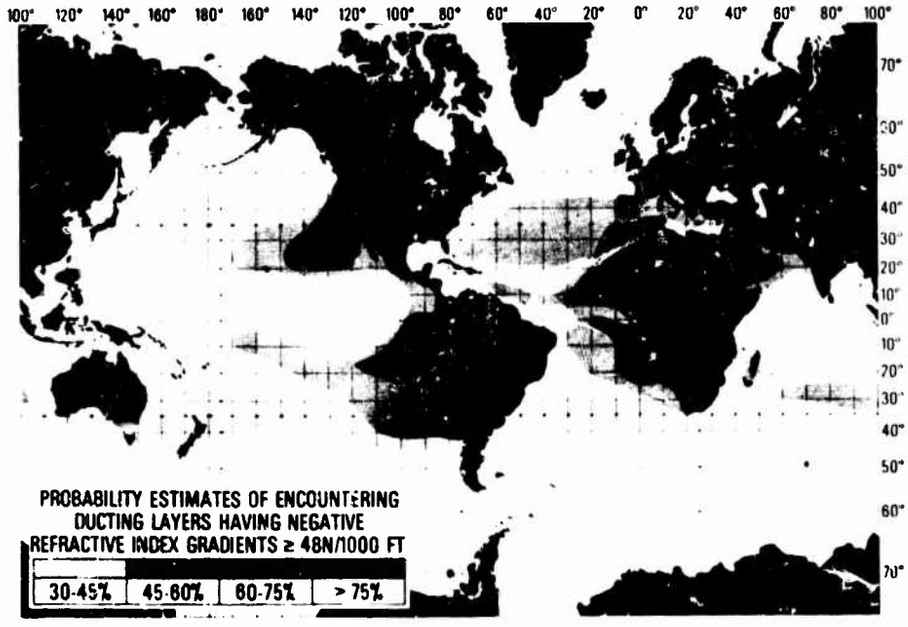

(b) August

Fig. 3 — Regions of persistent oceanic atmospheric duct layers

photography gave indications of high persistent trapping layers. The analysis of the probability estimates greater than 50% is subjective and is based on the interpretation of cloud satellite photography data gathered over a period of more than 4 years and the high correlation of cloud-type and ducting conditions observed during extensive research investigations in trade wind areas.

ANOMALOUS PROPAGATION

Refraction effects, such as those associated with an elevated duct layer, especially for radars scanning within a few degrees of the horizon, have both favorable and unfavorable military operational significance. The extended ranges resulting from ducting, at times hundreds of miles beyond the normal radar horizon, can be useful in the early detection of targets that under normal refraction conditions would not be seen. This favorable aspect of early target detection via an elevated duct layer is also characterized by a radar hole above the duct; consequently, radar targets within the radar hole go undetected. The presence of a radar hole can be either favorable or unfavorable from a military point of view. The favorable aspect is the ability to stay in the radar hole to avoid detection by enemy radars. The most important factor, from a strategic combat point of view, is to be aware that both a duct layer and a radar hole exist and to use this knowledge advantageously whenever possible. Many military operational radar systems scan at preset ranges; the operator can switch from say a 200-mi sweep display to a 100-, 50-, and 10-mi display and follow the target as it moves closer to the observing radar. This aspect is fine in terms of giving an enlarged display much like a zoom camera lens. However, under ducting conditions, targets may be coming from multiple distances beyond that indicated on a fixed-sweep display scope. When this happens, false interpretation of the individual radar target returns occurs, which in the past has caused mock battle situations where long-range naval guns have fired at nonexistent targets beyond the visual line-of-sight ranges. To avoid such situations, a radar must be able to discriminate between real and false ranges, a task that can only be done by measuring the travel time to each target and showing the true ranges of each target displayed on the radar scope without ambiguity.

When anomalous propagation conditions such as ducting occur, it has been shown that a negative refractive index gradient greater than or equal to $48N$ units per 1000 ft exists. What has not been discussed are examples in nature that cause the trapping gradients. In general, when there is a significant moisture discontinuity, temperature inversion, or a combination of both, a corresponding density and refractive index gradient results. Meteorological conditions that cause trapping gradients are often related to such things as large-scale subsidence, cloud formations, haze layers, divergence, gravity winds, advection, and evaporation.

Large-scale subsidence, or slow sinking of air, is associated with high-pressure areas. Over the oceans, large high-pressure cells may remain stationary for long periods of time. Typical weather associated with the center of large oceanic high-pressure cells is usually clear skies, light winds, and good visibilities except in low-level haze or fog layers. The general sinking of air from high altitudes results in adiabatic heating due to compression, and a decrease in moisture content. Normally, air temperature decreases with height at an approximate rate of 2° C per 1000 ft. The adiabatic heating produced by the sinking air

produces a body of warmer and drier air above a lower cooler and more moist layer, and a temperature inversion results. Within the sinking air above the temperature inversion the temperature lapse rate approaches the dry adiabatic lapse rate of 3°C per 1000 ft, which gives an effective excess warming rate of about 1° C per 1000 ft as it descends. For example, an air parcel descending 10,000 ft at the dry adiabatic lapse rate would be 10° warmer than a similar air parcel that descended at the standard lapse rate. A temperature inversion is characterized by an increase of temperature with height. The warmer and drier air overriding the cool moist air below the temperature inversion results in a sharp density discontinuity that often produces strong ducting refractive index gradients along the interface of the temperature inversion. If sufficient mixing occurs in the moist marine stratum below the temperature inversion, a stratus cloud layer will form at the base of the temperature inversion. The stratus clouds are stable and have very weak vertical development; hence, they stratify and spread out along the base of the temperature inversion, which acts as a suppressing lid that inhibits vertical cloud development as long as the temperature inversion persists. Often when the temperature inversion occurs below the gradient level, the normal cloud-base altitude, which is usually in the 1500- to 2500-ft range, condensation in the form of visible moisture or clouds does not take place because of insufficient vertical lifting. When this is the case, a haze layer is often observed in the air below the temperature inversion. Figure 4 illustrates this case as obtained from airborne meteorological records.

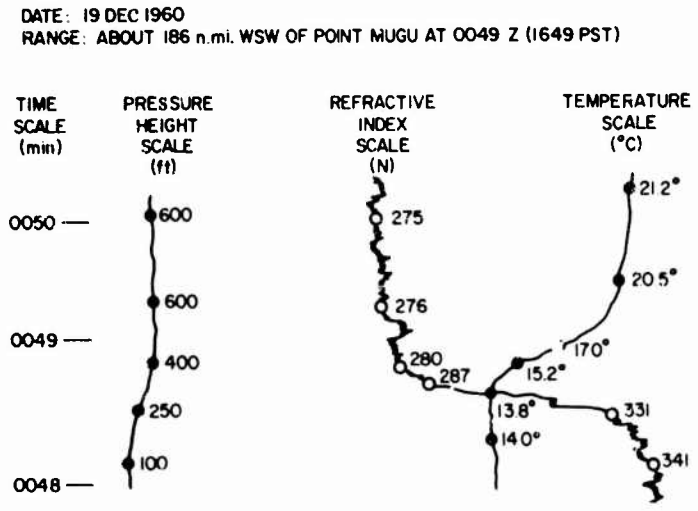

Fig. 4—Airborne meteorological recordings through a low-level elevated layer associated with a visible haze layer in a cloudless sky

In the sensing of the three meteorological parameters shown in Fig. 4, the microwave refractometer trace is much broader and more jittery than the other traces because of its faster response time. To get a more comprehensive evaluation of how the significant meteorological parameters and the refractive index gradients are changing, five points were selected from Fig. 4 and examined in closer detail. By making use of Eq. (14) and other acceptable proven meteorological mathematical relationships, we can see how the moisture parameters of vapor pressure e, dew point t_{DP}, and relative humidity RH were also changing. Table 4 shows these values.

Table 4
An Evaluation of Significant Meteorological Parameters in a Haze Layer

Point	Pressure Height (ft)	Pressure P (mb)	Temperature t (°C)	Dewpoint t_{DP} (°C)	Vapor Pressure e (mb)	Relative Humidity (%)	$t - t_{DP}$ (°C)	Refractive Index N	ΔN	ΔPH	$\frac{\Delta N}{\Delta H} \times 10^3$
1	600	991	21.2	- 8.7	3.183	13	29.9	275			
									5	200	- 25
2	400	999	15.2	-11.7	2.497	14	26.9	280			
									7	50	-140
3	350	1000	14.0	- 6.6	3.714	23	20.6	287			
									44	100	-440
4	250	1004	13.9	11.1	13.167	83	2.8	331			
									10	160	- 62
5	90	1010	14.2	13.2	15.120	93	1.0	341			

As can be seen from Table 4, the temperature inversion was over 7° C. The dramatic change in relative humidity from 83% at the base of the temperature inversion (250 ft) to 23% at 100 ft above and to 13% at the 600 ft PH level illustrates how much the subsiding air is dried out as it descends. The lower marine stratum, characterized by the visible haze layer, has relative humidity values in the 83% to 93% range. The temperature depression difference $t - t_{DP}$ between the dry air temperature and the dewpoint temperature has a minimum of 1.0° C in the haze and reaches a maximum of 29.9° C just a few hundred feet above the base of the temperature inversion. From 400 to 600-ft PH a superrefractive index gradient of -25 *N* per 1000 ft is observed. Below 400-ft PH, a negative trapping refractive gradient greater than 48*N* per 1000 ft is observed. Unfortunately, the aircraft could not safely go lower than 90-ft PH, so the refractive index gradient below 90-ft PH is unobtainable. However, the evaluation of the haze layer from 250- to 90-ft PH implies that a trapping gradient may well exist. This gives rise to the general hypothesis that oceanic evaporation (surface) ducts, which are generally believed to be quite shallow and normally less than 100 ft thick, may feed or be part of a low elevated duct layer that is sometimes characterized by visible haze. The general ducting concept for surface oceanic evaporation ducts is that it is not particularly effective in extending the coverage of most shipboard radars because it is too shallow to trap most radar frequencies below 3000 MHz, or wavelengths greater than 10 cm. As can be seen by the wavelength dependence criteria for trapping shown in Table 2, most shipboard operational radars having frequencies greater than 300 MHz, or wavelengths less than 100 cm, would have been able to trap energy into this duct layer.

On this particular research flight to observe meteorological and refraction conditions along the route from Honolulu to Point Mugu, the pilot's VOR was tuned to Santa Catalina on a VHF setting of 111.6 MHz at a range of 900 n.mi. Loud and clear audio signals were received, indicating the existence of a strong elevated duct layer. The best reception of the audio signal was received from an altitude just skimming the cloud tops to one 100 to 200 ft below the cloud tops. At the center of the interface of the temperature inversion, which occurred about 100 ft above the cloud tops, the audio signals would cut out sharply. Several probes above and below the overcast stratus cloud layer, whose cloud tops were at 4300-ft PH and bases were at 3300-ft PH, resulted in loss of signal just above the cloud tops and again at the cloud-base level. This showed agreement with the meteorological data because the duct and cloud thicknesses were both about 1000 ft. The use of the audio VOR signal is an independent verification that reliable deductions can be made concerning expected duct heights, ranges, and thicknesses.

On this flight radar plan-position indicator (PPI) pictures were obtained from an experimental airborne 435-MHz matched filter radar (MFR). An interesting photograph, Fig. 5, was obtained by the MFR at a range of about 566 n.mi. from Point Mugu and an altitude of 400-ft PH during a routine meteorological sounding [13]. In this figure the range within the center ring is 10 n.mi., and the full range of the scope is 278 n.mi. At about 400-ft PH the approximate distance to the radar horizon is 21 n.mi. Consequently, the radar target returns are being propagated via the observed elevated duct layer. The very strong multiple targets extending the full sweep of the scope are in all probability mountainous terrain of the California mainland. Also seen in the photograph is an array of targets along a common azimuth that extends about 150 n.mi. in length. It is believed that this may represent the width of the duct from the aircraft's position along the azimuth displayed by the targets.

Fig. 5—Target returns from beyond the radar horizon via an elevated duct layer using a 435 MHz MFR system [13]

At 566 n.mi., a target on the MFR scope could appear either at the maximum range limit of 278 n.mi., which is the end of the second repetition period, or on the center circle ring at the start of the third repetition period (i.e., 10 + 278 + 278 = 566). Consequently the position of targets in close proximity of 566 n.mi. on the MFR scope may be erroneously interpreted. For example, consider the case of two targets, A and B, that are actually only 20 n.mi. apart where target A is at a true range from the aircraft of 550 n.mi. and target B is 570 n.mi. from the aircraft along the same azimuth. The representation of target A would then appear on the MFR scope at a range of 262 n.mi. and would be in the second repetition period (i.e., 10 + 278 + 262 = 550). Target B would appear at an apparent range of 4 n.mi. from the 10-n.mi. center circle on the MFR scope and would be in the third repetition period (i.e., 10 + 278 + 278 + 4 = 570). Consequently, the representation of targets A and B on the scope would falsely indicate the range difference between them as being 288 n.mi. when in reality they are 20 n.mi. apart. Other range ambiguities may also result when target reception occurs from any other possible repetition period.

An NRL aircraft, during a 1960 Tradewinds III experiment, successfully recorded continuous signal-strength measurements via an elevated duct layer from a ground-based radar at San Diego for a range of 2400 n.mi. to a point about 150 n.mi. past Honolulu, where the flight was terminated because of the range of the aircraft. The significance of this particular flight is to show that certain geographic regions of the world, where persistent ducts are observed, are capable of trapping electromagnetic waves and transporting them in an effective atmospheric waveguide, not for a few hundred miles beyond the normal radar horizon but for several thousands of miles.

Detection of an atmospheric duct layer by audio VOR signals, when beyond the normal radar horizon range for reception, can be correlated with visual cloud and haze layer conditions and can be used to obtain independent estimates of duct height, range, and thickness. By using more than one VOR station, if possible, further estimates of

duct widths may be made. In the absence of meteorological refractive index data, it appears that audio VOR signals can provide an independent means for locating and describing significant characteristics of a duct layer. The same can be said of certain airborne radar systems such as the MFR.

It should be noted that most radar systems were designed to take into consideration the estimated range to the horizon for normal atmospheric conditions and normal aircraft ceilings. For example, an aircraft at 40,000 ft would expect to have a radar horizon range of about 213 n.mi. This explains why the typical range of operational radars is about 200 n.mi. One approach to remove target range ambiguities in surface and elevated duct regions where the target return ranges exceed one repetition period would be to change the pulse repetition frequency (PRF) slightly. A switching back and forth at different PRFs would see no range changes of targets in the first repetition period. For targets beyond the first repetition period, the change in PRF would help identify targets of ambiguous ranges as they would not appear at common ranges for each of the PRF switch settings.

Until now the approach in obtaining a RIF has been by use of existing synoptic meteorological services where a forecaster would use whatever atmospheric data is available to him and by standard procedures make a forecast. This approach is still desirable; however, there are many additional aids to obtaining a RIF such as from aircraft radars, as already mentioned, plus the use of satellite cloud photographs where a correlation of clouds and ducting layers may exist. By bringing to light some of the alternative methods not readily found in the literature of obtaining a RIF, we hope that it may be possible for operational personnel in the field to obtain a RIF when the standard forecasting service approach is unobtainable.

During a February 1961 Tradewind IV meteorological research flight over the Honolulu to San Diego route, a series of photographs of the MFR scope was obtained above, in, and below an elevated duct layer. A selection of 12 radar scope photographs [14] showing transhorizon radar returns associated with an elevated duct layer is presented in Fig. 6.

During the 4.5-min span of the 12 photographs, the aircraft descended from 2660- to 560-ft PH and the range from San Diego changed from about 542 to 527 n.mi. The radar scope pictures not only substantiate the presence of an elevated duct layer but clearly illustrate how target reception is affected in close proximity of the elevated duct layer. During this flight the Navy Electronic Laboratory (NEL) at San Diego recorded signal-strength measurements of the aircraft's 435-MHz MFR. A continuous duct layer, associated with a strong haze and thin scattered-to-broken stratus cloud layer, showed excellent correlation with the microwave refractive index measurements and the recording of the radar signal-strength measurements. The first detection of this continuous duct layer by the NEL measurements occurred at a range of 1320 n.mi. In the last 550 n.mi. of this flight there was nearly lossless propagation with peak signals measured in the 25- to 30-dBm range. Photograph 1 in Fig. 6 was taken about 600 ft above the cloud tops and about 450 ft above the top of the duct as determined by refractometer data and visual cloud observations. Here a faint but persistent target in the direction of flight (2 o'clock) is seen coming, presumably from the San Diego area. In the remaining photographs the returns at 11 o'clock are presumed to be coming from the San Francisco area and the returns at 4 o'clock from Guadalupe Island. The azimuth spread

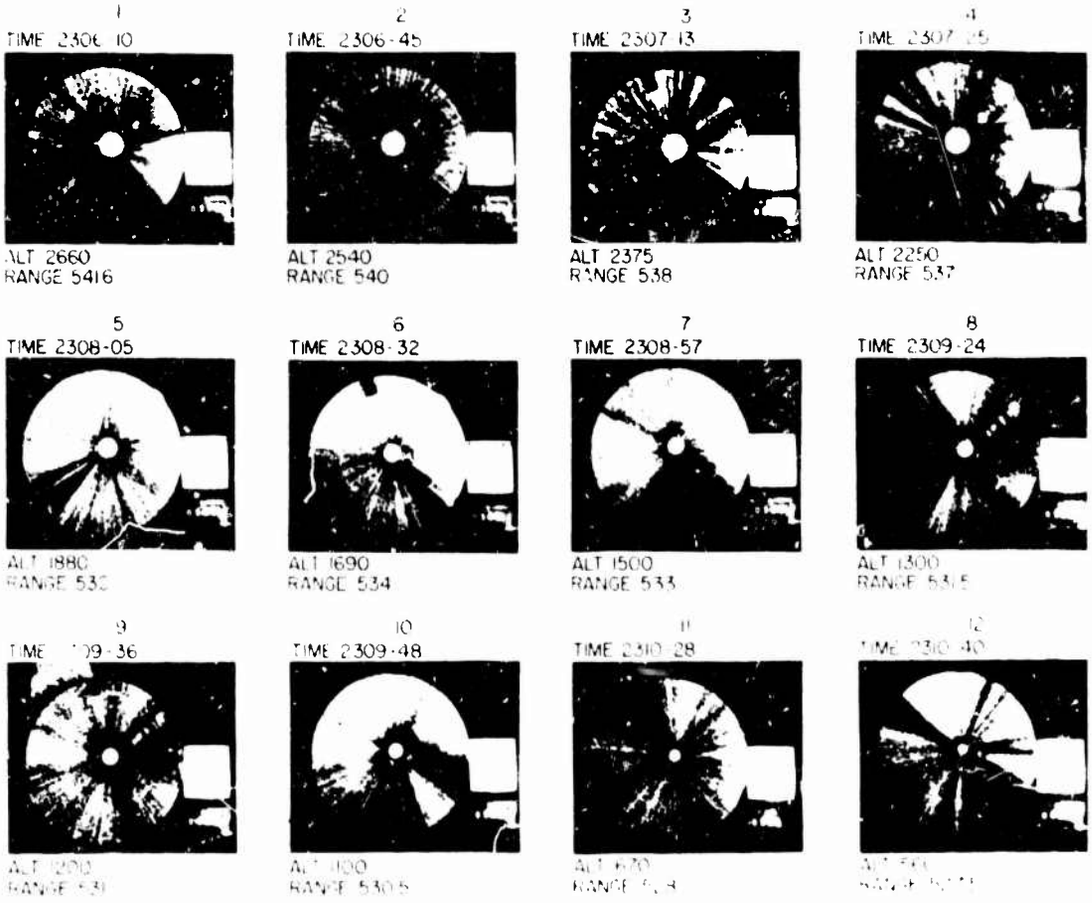

Fig. 6 — Radar scope pictures associated with an elevated duct

of these targets is an indication that the duct is quite broad. Photographs 2 and 3 show slightly brighter illumination of the San Diego area targets and detection of targets from the San Francisco area. At the time of these photographs the aircraft was in clear air about 200 to 300 ft above the duct base. Photograph 4, taken within 50 ft of the duct top, shows many more returns from the San Diego area and a significant increase in illumination. Photographs 5, 6, and 7 were obtained within the duct layer, and the targets show a high illumination, which indicates that the signal strength is greatest within the duct layer. This agrees with the recorded signal-strength measurements that gave a peak reception power of 25 to 26 dBm when the aircraft was between 1900 and 1000 ft. Photograph 10 was taken at 1100 ft, about 1150 ft below the duct top, and shows the San Diego returns to be fain although the San Francisco and Guadalupe Island returns are somewhat stronger. Photograph 12 was taken at 560 ft, or about 1700 ft below the duct top, and shows no target returns. The minimum detectable signal-strength level for the 435-MHz MFR occurs near 100 dBm. Consequently a drop of about 80 dB, or more, is associated with the change from the peak signal strengths within the duct layer to the loss of signal below the duct layer.

CORRELATION OF ELEVATED DUCTS WITH CONTINUOUS CLOUD HAZE LAYERS

From March 1959 to November 1961 NRL conducted four major meteorological ducting experiments in trade wind areas. Tradewinds I and II took place over the Recife, Brazil to Ascension Island route in the South Atlantic Ocean and were conducted in March and November 1959, respectively. Tradewinds III and IV took place over the San Diego to Honolulu route in the North Pacific between July 1960 and November 1971. During these experiments, extensive atmospheric measurements of radar signal field strength, microwave refractometer profiles, and other significant recorded and visual meteorological data were simultaneously obtained in close proximity to observed elevated duct layers. During the South Atlantic experiments, NRL was the first to track and make continuous measurements of radar signals via an elevated duct at distances over 1000 n.mi. Over the longer North Pacific trade wind route, successful tracking of continuous radar signal measurements was performed to a range of 2400 n.mi. One of the most significant meteorological findings related to the trade wind inversion was the apparent correlation noted between the extent of continuous radar signal ranges via an elevated duct layer and the extent of continuous cloud haze layer conditions. Table 5, obtained from the 14 transits between Recife and Ascension Island made during the Tradewinds II experiment, contains data on the altitudes of continuous radar signal ranges and continuous cloud haze layers for such a comparison.

Table 5
A Comparison of Continuous Radar Signal Ranges With Continuous Cloud Haze Layer Conditions

Mission Number	Continuous Radar Signal Range (n.mi.)	Continuous Cloud-Haze Layer (n.mi.)
1	500	540
2	540	540
3	750	700
4	700	710
5	950	950
6	540	530
7	1100	1090
8	1000	1120
9	520	500
10	550	500
11	750	540
12	850	1110
13	500	500
14	600	540
Average	704	705

During the Tradewinds II experiment [15], the radar signal measurements were made air-to-air between two naval aircraft. A transmitter, operating on a 220-MHz frequency with a nominal CW output of 90 W was carried at the inversion altitude by an aircraft

that flew a racetrack pattern 100 n.mi. off the beach at Recife. The receiver was carried at the inversion level by another aircraft flying along the 1200-n.mi. route to Ascension Island. It is interesting to note that the transmitted air-to-air signals were propagated the maximum range between the two aircraft on 3 of the 14 flights. Using the range values shown in Table 5 results in a high correlation of $r = 0.92$ when comparing the ranges of the continuous radar signals with the continuous cloud haze layers.

Further data that correlated the extent of radio signal experiments with the extent of continuous cloud haze layers was noted during the North Pacific Tradewinds III and IV experiments. These experiments were conducted between San Diego and Honolulu during 1960 and 1961 in a trade wind area where temperature inversions are persistantly found stronger than those measured along the Recife to Ascension Island route. Data from 41 flights between San Diego and Honolulu indicated that the average range for both the continuous radar signals and continuous stratus clouds and haze layers was about 1000 n.mi. From a climatological point of view, it is interesting to note that continuous stratus cloud formations extend as far as they do. During the summer months the average extent of continuous stratus clouds was about 1280 n.mi. compared with the annual average of about 905 n.mi. The statistics using the 41 North Pacific flights gave the same correlation of $r = 0.92$ that was obtained in the South Atlantic.

A comparison of the extent of continuous stratus clouds with observed radar signal-strength measurements in an elevated duct layer and the corresponding ray-tracing profile is presented in Fig. 7.

The four diagrams shown in Fig. 7 are aligned with a common range scale. Zero distance represents the location of San Diego. The four diagrams depict the visual cloud formations, the observed radar signal-strength measurements, the ray tracing profiles, and the aircraft's flight altitude. It should be noted that no signal-strength measurements were recorded within 350 n.mi. of San Diego because of ground station equipment failures. In addition, the ray-tracing diagram is arbitrarily depicted for the case where the antenna is placed at the cloud-top level at the start of the stratus overcast layer. Gaps in the received signals occur at times because of the inability of the ground station personnel to keep the antenna pointed directly at the aircraft. Between 400 and 500 n.mi., the received signal sharply drops and then peaks at about 30 to 50 dB as the aircraft climbs out of and back into the duct layer. If the signal fluctuations during the times the aircraft was out of the elevated duct layer are ignored, the significant feature displayed by the radar signal-strength measurements is the observation that the maximum received signals show little or no losses to 1200 n.mi. During this portion of the route, the elevated duct layer is associated with the slowly rising stable stratus cloud layer, which acts as an efficient waveguide. In previous trade wind flights, significant attenuation of the received radar signals had occurred with a rapidly rising cloud layer. Between 1200 and 1380 n.mi. there was a significant rise in the slope of the stratus cloud layer and approximately 30 dB attenuation in signal strength. The loss of signal at 1380 n.mi. agrees with the correlation of continuous radar signals and continuous stratus clouds.

The ray-tracing diagram was obtained by electronic computer analysis and automatic plotting techniques using the refractive index measurements obtained during the flight to determine the ducting or bending characteristics over the propagation path. In the computer analysis, 45 pencil rays were launched at a range of 300 n.mi. and a height of 1300 ft. A half-milliradian interval (about 0.03°) was used between the limits of ±11 mrad (±0.63°) from an axis parallel with the horizon. The first three rays, 11, 10.5, and

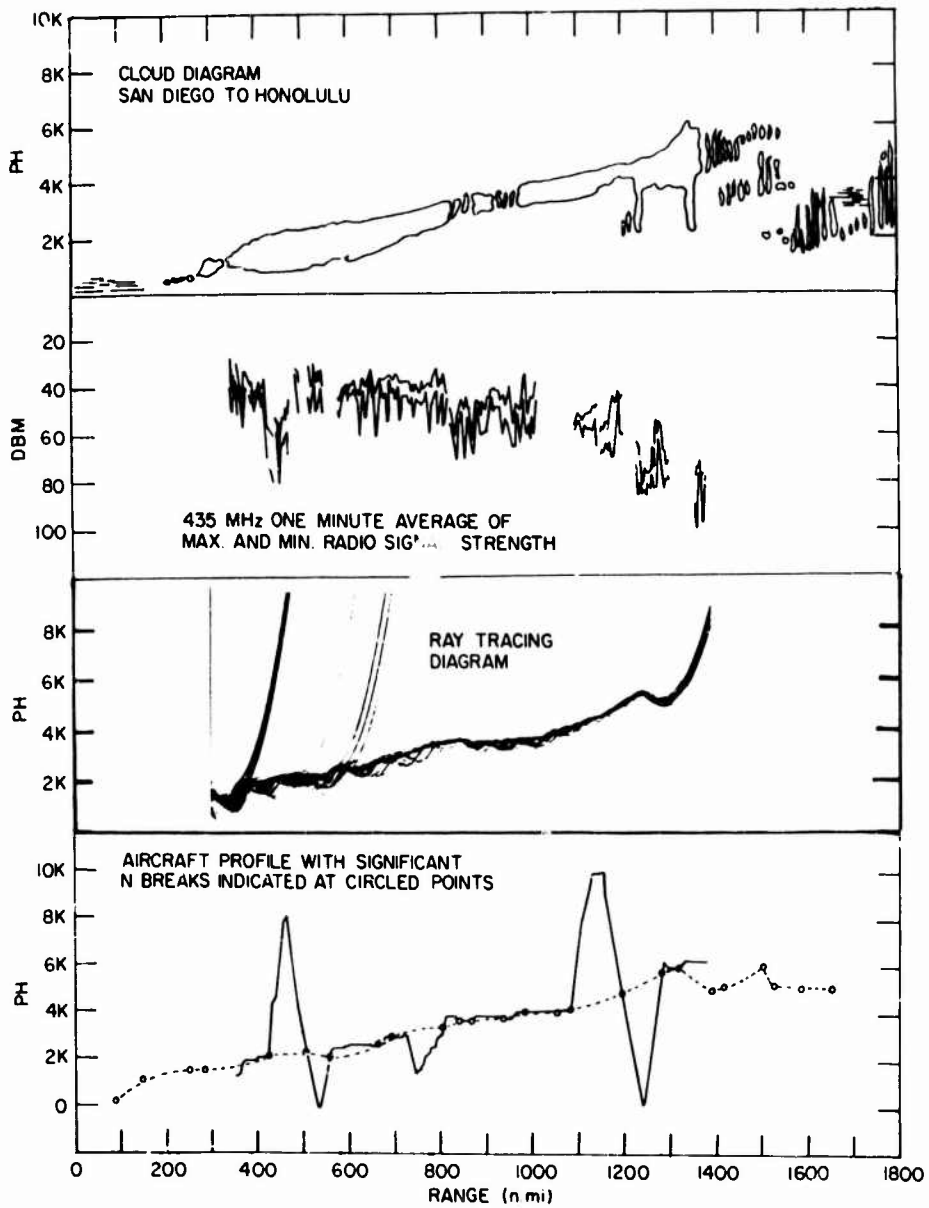

Fig. 7—Comparison of the extent of stratus clouds with radio signal measurements and ray-tracing analysis (Tradewinds IV, mission 5, February 21, 1961)

10 mrad (+ 0.63° to + 0.57°), were too steep to be trapped in the duct. The last nine rays launched between -7.0 and -11.0 mrad (-0.40° to -0.63°) were also too steep to be trapped in the duct layer. The first ray trapped in the duct was launched at an angle of 9.5 mrad (+0.54°), and the last ray trapped in the duct layer was launched at an angle of -6.5 mrad (-0.37°). Therefore, the angular spread for the 33 rays trapped in the duct was 0.91°. Consequently, of the 45 rays launched, only 33 were trapped in the elevated duct layer. If one considers the number of rays lost or escaping the duct layer as being proportional to the power lost, then the following mathematical relationship should exist:

$$\text{the total decibel loss} = 10 \log_{10} \frac{\text{total rays trapped} - \text{total rays lost}}{\text{total rays trapped}} . \qquad (34)$$

For the example in Fig. 7 where 33 of the 45 launched rays were trapped in the elevated duct layer, two rays escaped at 225 n.mi. from the launch point (525 n.mi. on the range scale) and eight more rays leaked out between 300 and 250 n.mi. from the launch point (600 to ~650 n.mi. on the range scale). Consequently, the decibel loss for the case of 33 trapped rays when 10 rays escaped the duct, as determined by Eq. (34), would be -1.8 dB. This loss rate shows excellent agreement with the measured signals for the 900 n.mi. between the 300-n.mi. launch point and the 1200-n.mi. point where the stratus layer and duct interface layer immediately above the cloud tops were rising very uniformly. The resultant 30-dB peak power loss from 1200 n.mi. to 1380 n.mi. is associated with the sharp rise in the slope of the stratus cloud layer and the end of the continuous stratus cloud and related elevated duct layer.

CORRELATION OF CLOUD TYPES WITH SIZE OF TEMPERATURE INVERSION

The trade wind inversion, perhaps the most important regulating valve of the general circulation, was first discovered in 1856 by C. Piazzi-Smyth during an astronomical expedition in the Canary Islands. His detailed measurements taken while climbing up and down a mountain peak revealed a marked temperature inversion associated with a sharp decrease in moisture content. Also noted at the time was a visual correlation between the tops of the cloud layer and the temperature inversion. The first large-scale atmospheric exploration of the trade wind inversion occurred in 1926 during the 2-year German Meteor Expedition in the cold-water strip near the African West Coast. From numerous kite soundings taken in the North and South Atlantic trade wind areas, the German scientist Von Ficker [16] published what is now considered the classical treatise on trade wind inversion. Some of the more significant findings of the expedition concern the areal distribution of the heights and magnitude of the temperature inversions. The extensive worldwide aircraft radar meteorological investigations of elevated duct layers in trade wind areas conducted by NRL between 1959 and 1962 represent a major contribution to knowledge of the causes and effects of trade wind inversions, about which much is still to be learned.

A better understanding of radar atmospheric propagation effects caused by the trade wind inversion is obtained by evaluating some of its significant large-scale features. From the German Meteor Expedition and NRL experiments, one of the key observations is the relationship that exists between the height and size of the temperature inversion. These two factors have a direct relationship to visual cloud patterns and continuous

electromagnetic wave propagation beyond the normal radar horizon via an elevated duct layer. The comparison of trade wind inversion heights in the downstream range direction from the west coasts of Africa and the United States where the inversions originate is shown in Fig. 8.

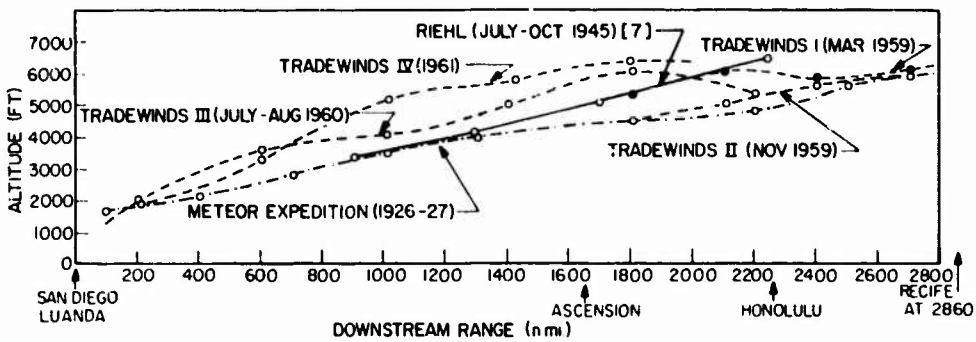

Fig. 8—Comparison of trade wind inversion heights

It is interesting to note, from Fig. 8, that even though the two routes are oceans and hemispheres apart in geography and the data a generation different in time, trade wind height slopes are quite similar. A plot of an average height curve would give an approximate mean slope rise of about 230 ft per 100 n.mi. for the heights of the trade wind inversion between 2000 and 5000 ft.

From 5000 to 6000 ft the mean slope flattens out to an approximate rise of 100 ft per 100 n.mi., or less than one-half that observed below 5000 ft. As has been previously discussed, the top of the cloud layer and the base of the duct interface coincide with the base of the temperature inversion. Consequently, the trade wind inversion height can also be identified with the heights of the cloud tops that are normally being suppressed by the temperature inversion. During the NRL Tradewind Experiments, a significant observation correlated cloud type with the size of the temperature inversion. Figure 9 illustrates this relationship.

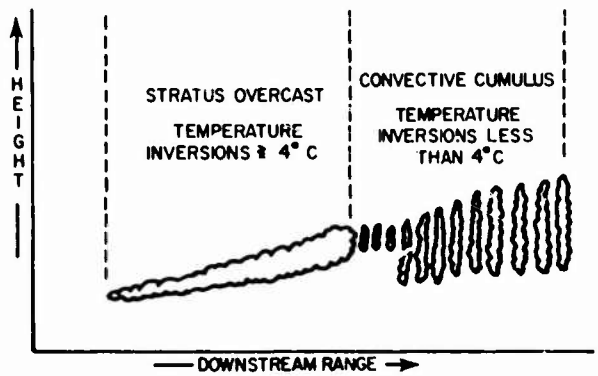

Fig. 9—Correlation of cloud type with temperature inversion size in trade wind areas

The last 10 flights of the Tradewinds IV San Diego to Honolulu route were carefully examined to determine the validity of the critical temperature inversion relationship to cloud type as depicted in Fig. 9. To remove ambiguity, only soundings or probes that went 1000 ft above the cloud tops were evaluated because during straight and level flight it is not possible to determine the full value of the temperature inversion size.

Out of 53 cases, 49 showed agreement with the critical 4° C temperature inversion-cloud type correlation. Three of the four cases that did not conform were within 400 mi of the California coast where the cloud tops were less than 2000 ft. These cases can be linked to large-scale meteorological conditions that create exceptions to the general correlation between cloud type and size of temperature inversion.

Quite often the continuous stratus overcast rises to heights of 4000 to 6000 ft or more and may exceed 1000 n.mi. in range before dissipating. Figure 10, obtained from actual flight records, shows three cloud diagrams with corresponding temperature inversion values immediately above the cloud tops. As can be seen in each of the cloud diagrams, once the continuous stratus layer has cloud tops over 2000 ft the temperature inversion remains greater than 4° C. At the end of the continuous stratus cloud layer there is a significant drop in the size of the temperature inversion and the clouds become more convective. It should also be noted that the three diagrams are winter month cases in which the average maximum range to the end of the stratus layer is about 1200 n.mi., or better than one-half the distance along the San Diego to Honolulu route. Figure 10b also shows a rather steep height slope of about 833 ft per 100 n.mi. for the cloud top level, which is about three times steeper than the mean slope of the trade wind inversion shown in Fig. 8. In each of the three diagrams in Fig. 10, strong ducting refractive index gradients were continuously observed at the cloud top levels and the elevated duct layer was continuous to the end of the stratus cloud layer.

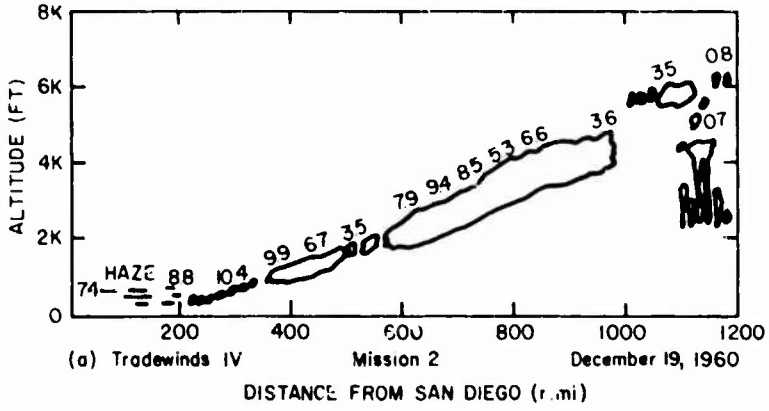

(a) Tradewinds IV, Mission 2, December 19, 1960

Fig. 10 — Examples of rising stratus cloud layers

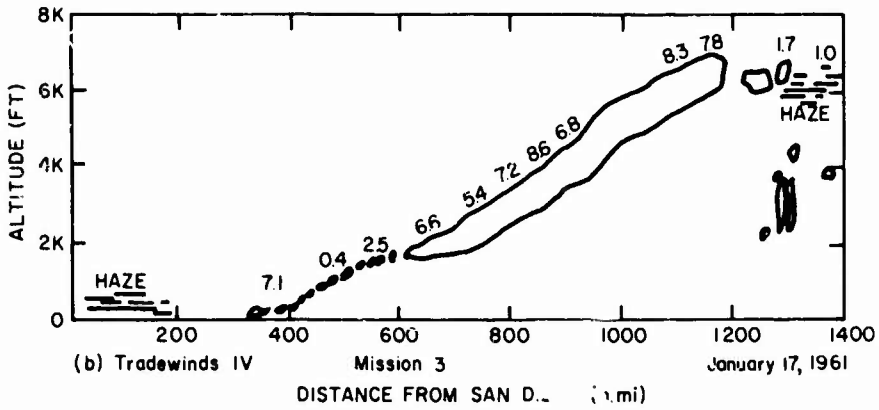

(b) Tradewinds IV, Mission 3, January 17, 1961

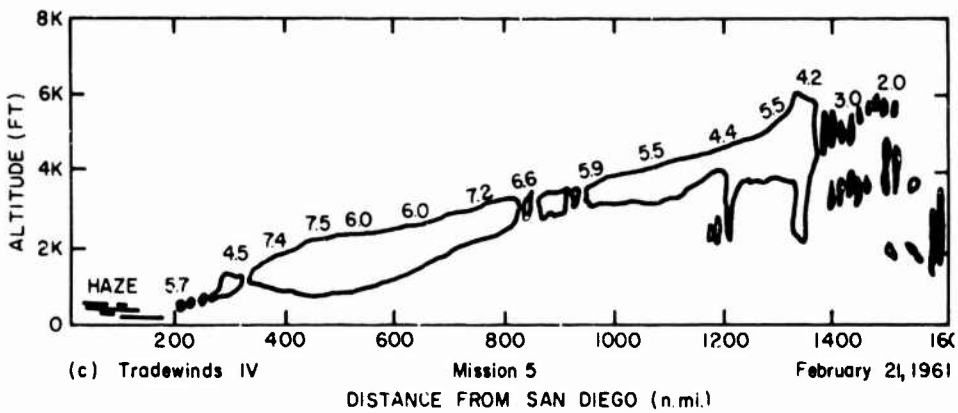

(c) Tradewinds IV, Mission 5, February 21, 1961

Fig. 10—Examples of rising stratus cloud layers (Cont.)

CONVECTIVE CLOUD CELLS

Numerous times during the NRL Tradewind flights, especially in the South Atlantic, a typical cloud pattern was observed when the temperature inversion approximated 2° C. In trade wind regions when there is a relatively weak but persistent temperature inversion, a distinctive visual cloud pattern occurs. An oval or circular clear area is ringed by an area of convective cumulus clouds. The size of these cells, sometimes referred to as Benard cells, may vary considerably depending upon conditions of large- or small-scale subsidence. In laboratory experiments using a fluid in which the viscosity decreases as temperature increases, the motion is upward in the center of the cells and downward at the edges. However, in a gas such as the atmosphere, the motion is downward in the center and upward at the edges. Figure 11 consists of two aerial photographs, obtained in December 1958 over Recife, Brazil by Dr. Robert Cunningham of the Air Force Cambridge Research Center, taken at about 25,000 ft that show evidence of the convective cell cloud pattern [18]. Figure 12a is a cloud mosiac taken from the second

(a)

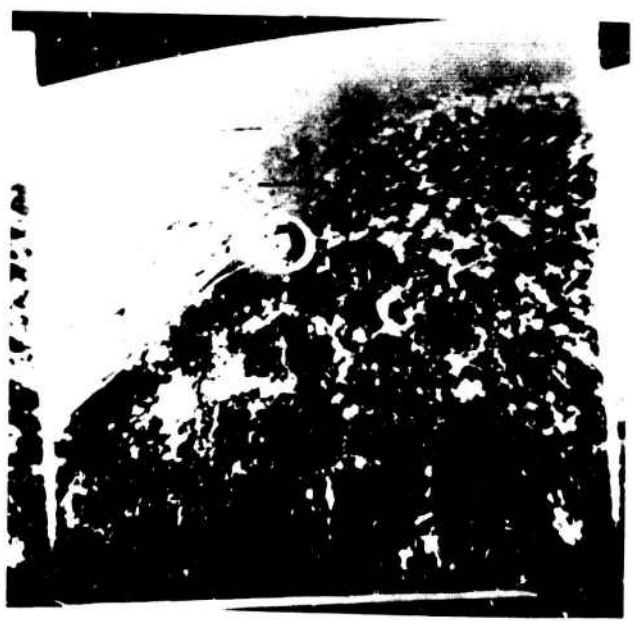

(b)

Fig. 11 — Aerial photographs of convective cells [18]

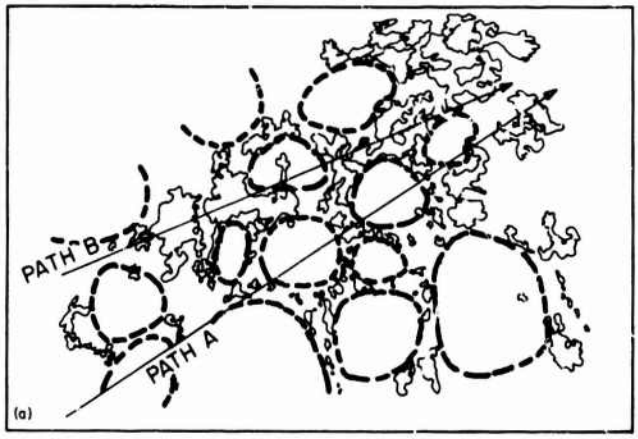

(a) Cloud mosaic from second photograph in Fig. 11

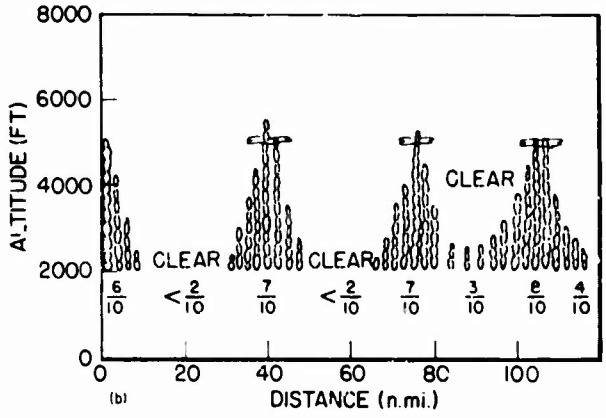

(b) Path A—route of minimum cloudiness

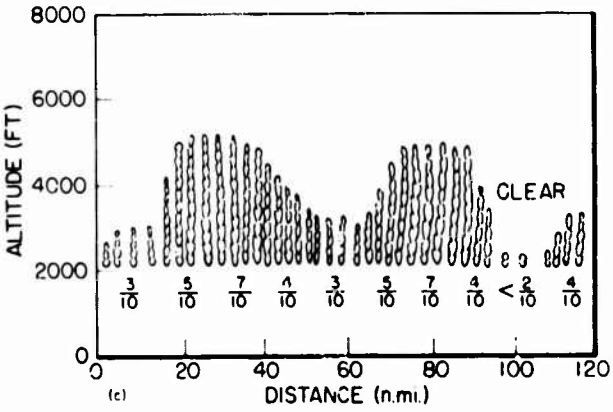

(c) Path B—route of maximum cloudiness

Fig. 12—Routes of minimum and maximum cloudiness in convective cell areas [18]

photograph in Fig. 11. Figures 12b and 12c illustrate the significant differences in cloud structure that exist along two adjacent paths [18]. Figures 11 and 12 illustrate the significant characteristics of convective cell clouds as related to electromagnetic wave propagation.

In Fig. 12, path A represents a route of minimum cloudiness and path B a route of maximum cloudiness close to path A. A typical cloud diagram depicting these two paths is shown in Figs. 12b and 12c. The ranges indicated on the cloud cross-section diagrams are based on visual observations and are considered to be representative. The areas of maximum cloudiness are related to areas of convergence resulting in vertical updraft motions. The clear areas are the result of subsidence and divergence and are related to sinking air from aloft, which causes the air to be warmer and drier than the surrounding air. Frequently these clear cells extend down to the sea surface, and it is interesting to note that the cloud heights are visually related to the inverted bulges, or clear cells, that permeate the area. When flying at low altitudes, it is very difficult to recognize these convective cells, as they must be seen from a high vantage point to be recognized as such. Compared to the continuous stratus cloud layers, propagation conditions through areas where convective cells commonly occur cannot be statistically documented in terms of the predicability of continuous propagation. However, the overall high frequencies of continuous and intermittent long stretches of received air-to-air radar signals observed over the Recife to Ascension Island route were many times propagated through large-scale areas of convective cells. In all probability it is reasonable to assume that better propagation conditions would result in a route of minimum cloudiness because a more cloudy route, such as path B in Fig. 12a, is subject to more unstable air, which because of increased vertical development is dissipating the intensity of the temperature inversion.

RAY TRACING USED TO EVALUATE ANOMALOUS RADAR PROPAGATION EFFECTS

There is little question that the state of the art in providing RIF's will be greatly enhanced by the use of digital and analog computers. Additional research is needed to provide adequately acceptable atmospheric models to improve the Navy's forecast capabilities. A graphic display of a family of rays emanating from a radar transmitter, showing the behavior of each pencil ray as it travels through space, certainly gives the operational analyst a more realistic picture of the causes and effects associated with anomalous radar propagation. Simple usable models have existed for over a generation that show very complex cross-sectional diagrams when using refractive index profiles obtained in nonstandard atmospheric conditions. With the advent of satellite photography, the meteorologists and cloud physicists are gaining a much better understanding of the relationship between basic cloud types and synoptic weather conditions. The use of the computer allows both the hypothetical and actual complex measured cases to be evaluated. Many aspects of radar propagation, such as ducting, radar holes, antiholes, irregularities in signal fluctuation, range and elevation angle errors, and the effects caused by the changing height of a radar transmitter are more readily evaluated by electronic computers.

During the NRL Pacific Tradewinds flights, there were cases in which a continuous stratus layer in the downstream direction would have gradual, steady, evenly rising slopes,

sudden abrupt increases in slope rates, no rise in cloud-top levels, and a decrease in cloud-top levels. As previously discussed, the more typical case was slowly rising cloud height, with a gradual increase in the downstream direction. The sudden abrupt increases in the cloud-top level were often associated with cases of either small- or large-scale convergence, such as those experienced when the strength of the temperature inversion weakened to less than 4° C and convective cumulus clouds pushed upward because of increased vertical motion as the trade wind inversion weakened. Another meteorological factor related to a sharp rise in cloud tops was associated with a high-pressure ridge. A leveling of the cloud tops was usually an indication of increasing subsidence, which would normally result in an increase in the size of the temperature inversion. The times that the cloud heights were decreasing in the downstream direction were usually when the stratus cloud tops were below 2000 ft, very thin in depth, and within a few hundred miles of the California coast. Usually in these instances the size of the temperature inversion was quite large, perhaps in excess of 10° C, and multiple haze layers were present above the cloud tops.

Several years after the NRL Pacific Tradewinds propagation experiments, an NRL Report 6253 [19] was published that showed ray-tracing examples for cases of rising and falling duct layers. The mathematic model used for the computer plots of the ray-tracing examples is fully explained in the report. Figures 13 to 16, published in Ref. 19 as Fig. 8 to 11, are presented to illustrate the value of using ray-tracing profiles in areas where anomalous radar propagation effects are associated with elevated duct layers.

SATELLITE CLOUD PHOTOGRAPHY USED FOR REFRACTIVE INDEX FORECASTING

French scientists Schereschewsky and Wehrle are noted for their analysis of weather based solely on cloud observations [20]. They developed a mapping of cloud systems in France as early as 1923. A correlation of visual cloud observations with frontal synoptic weather conditions, especially in areas where standard weather stations are very sparce such as in Africa, was successfully used as a supplemental forecasting technique. In more recent times a number of meteorologists have used correlation methods involving cloud patterns to explain large-scale synoptic weather. Today's professional forecasters are finding more ways of utilizing cloud information in local and large-scale weather forecasting.

The NRL Tradewinds experiments clearly indicate that a correlation exists between cloud types, temperature inversion magnitude, and propagation conditions via an elevated duct layer. Additional research of this type in other than trade-wind areas is needed to have a better understanding of this subject.

In the past, the visual observing of cloud information normally recorded on synoptic weather charts was far from ideal. However, the gross cloud picture could usually be identified with large synoptic weather patterns. The current weather satellite program offers a new observation technique capable of giving worldwide synoptic coverage of weather conditions. The continuing use of satellite cloud photography is resulting in more reliable and detailed cloud charts, which are helping to improve the state of the art in local weather forecasts. Satellite cloud photographs already give evidence of more large-scale organization of cloud patterns than previously had been conceived. The orientation of frontal bands, cyclonic swirls, and other organized patterns is so pronounced

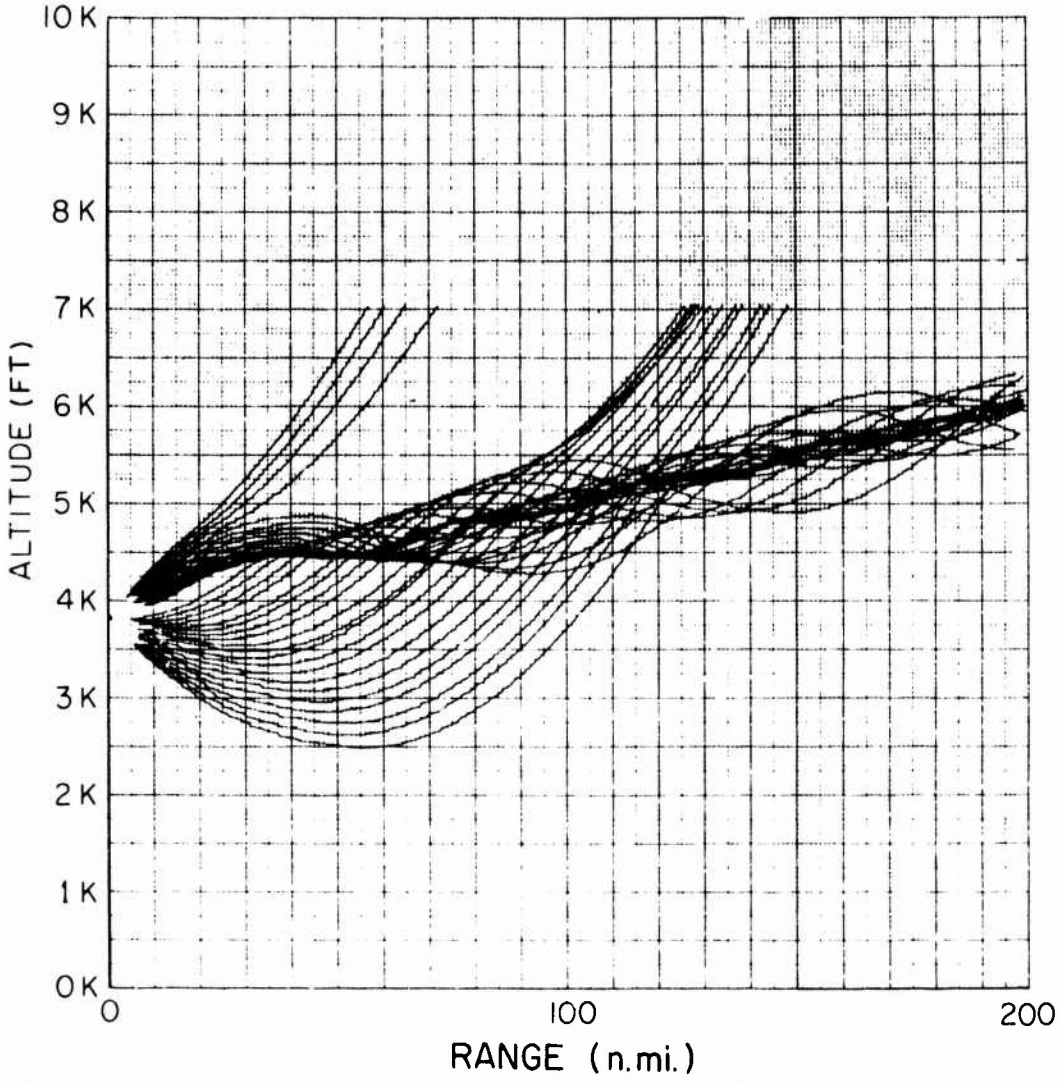

Fig. 13—Rising duct layer. Family of ray paths calculated for a 500-ft-thick interface with a slope of 1.89×10^{-3}, a gradient in the interface of -0.1 N units per foot, and a gradient above and below the interface of -0.01 N units per foot [19].

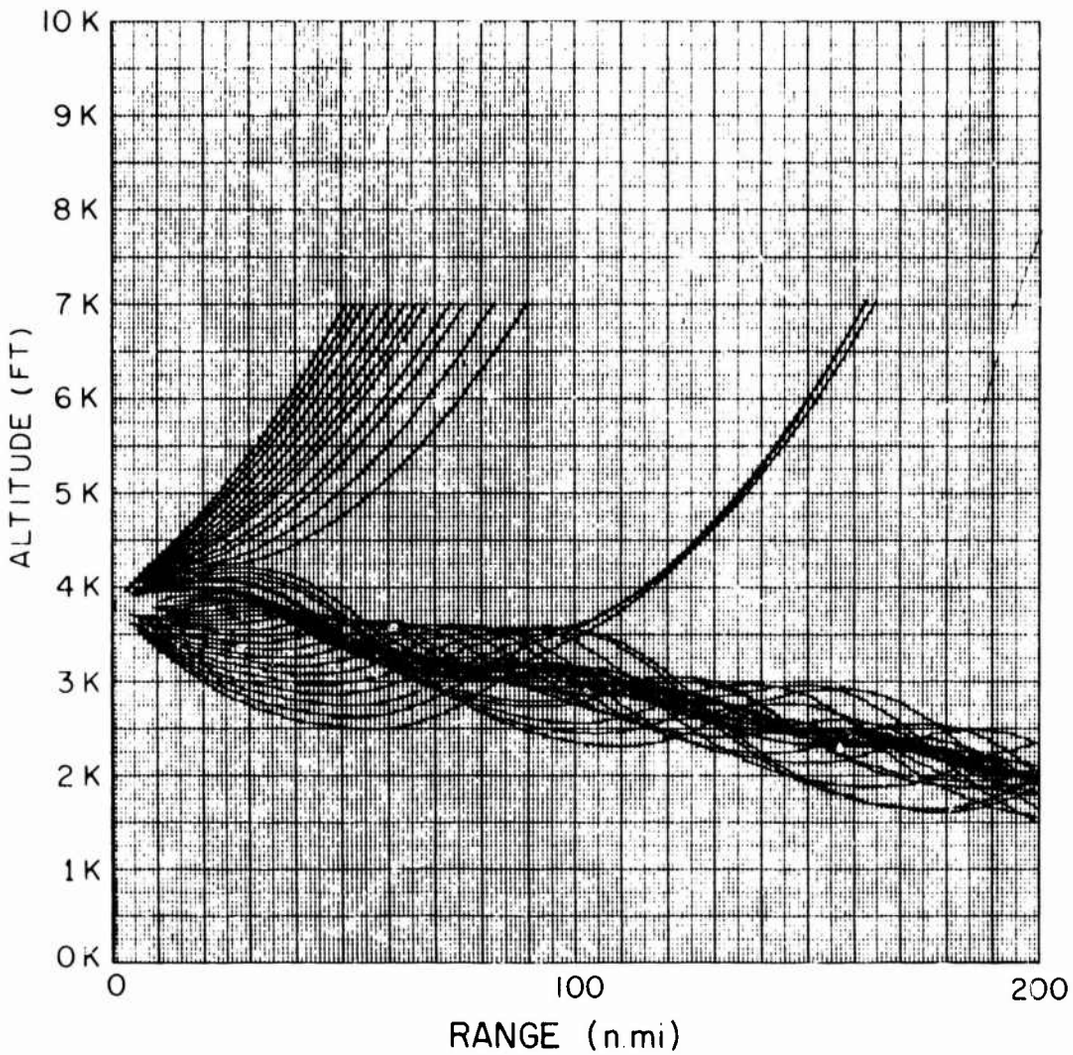

Fig. 14—Falling duct layer. Family of ray paths calculated for a 500-ft-thick interface with a slope of -1.89×10^{-3}, a gradient in the interface of -0.1 N units per foot, and a gradient above and below the interface of -0.01 N units per foot [19].

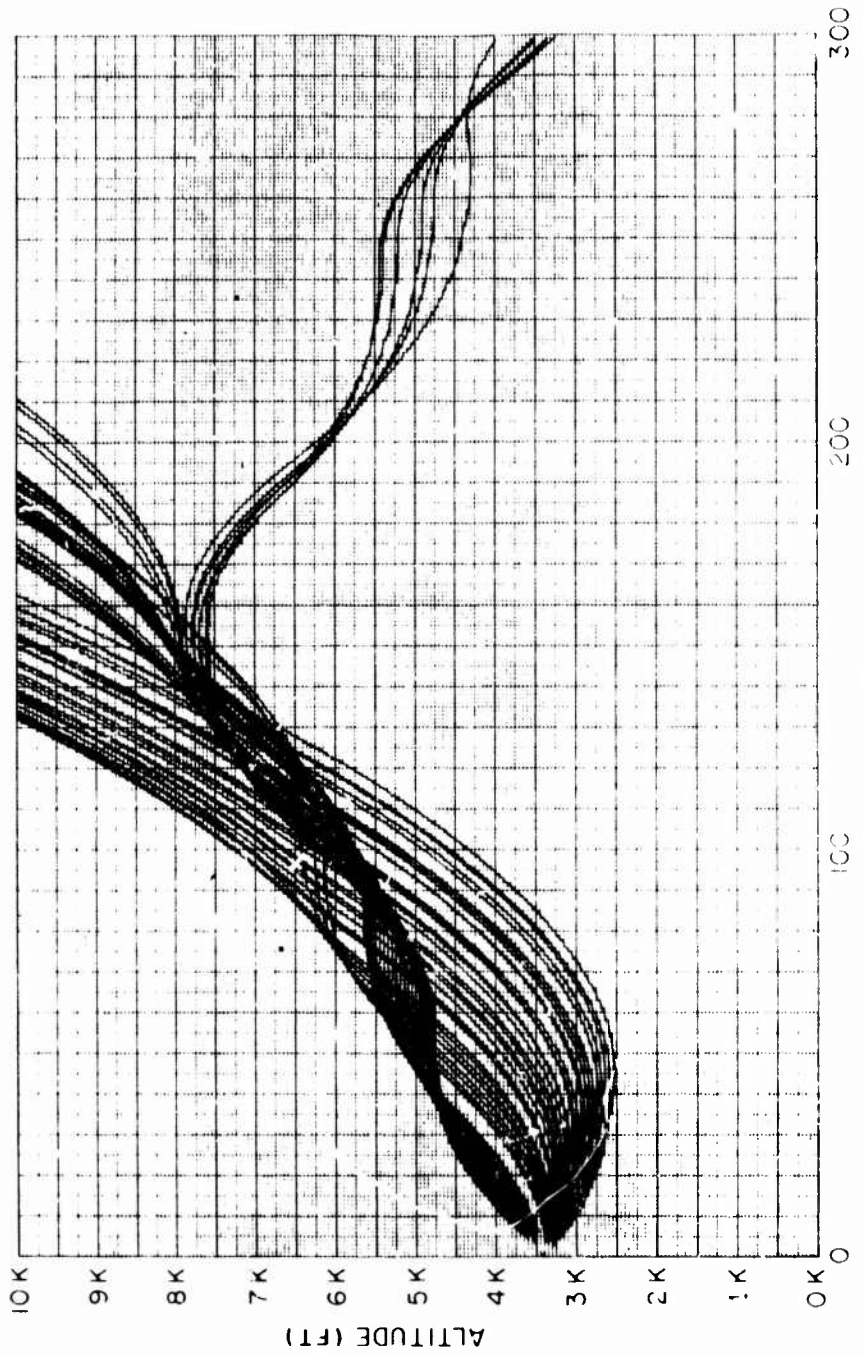

Fig. 15—Rising and falling duct layer. Family of ray paths calculated for a 500-ft-thick interface with a slope that changes at 150 n.mi. from 4.17×10^{-3} to -4.17×10^{-3}, a gradient in the interface of -0.1 N units per foot, and a gradient above and below the interface of -0.01 N units per foot [19].

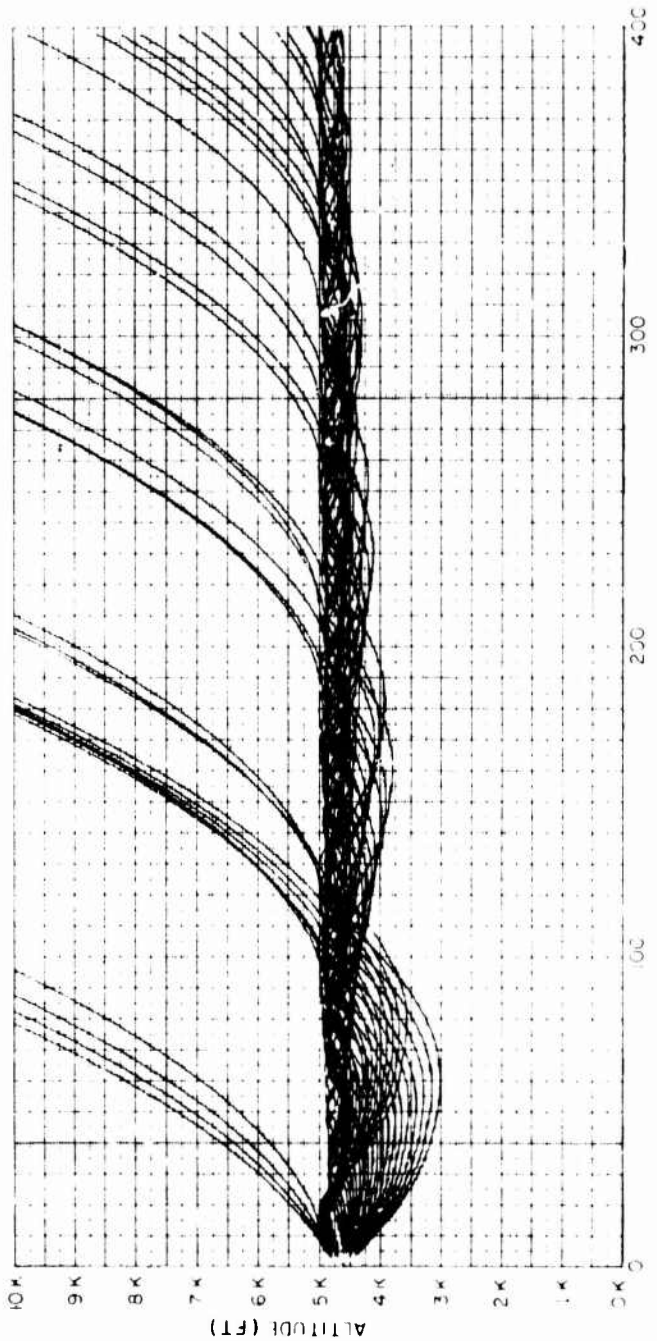

Fig. 16—A leaky duct layer. Family of ray paths calculated for a 500-ft thick horizontal interface, a gradient in the interface that changes linearly from 0.2 N units per foot at zero range to 0.05 N units per foot at 400 n.mi., and a gradient above and below the interface of 0.01 N units per foot [19].

in some instances that when it is correlated with the pressure gradient field, one has an immediate physical feeling for the accompanying circulation.

During the NRL Tradewinds experiments there was one case in which TIROS data were obtained simultaneously in the same area as the NRL aircraft flight data. This occurred during the time of the August 1961 Tradewinds IV flights. Prior to takeoff from Honolulu on August 25, 1961, an operational forecast was made through naval weather facilities for the extent of the continuous stratus overcast along the route to San Diego. On the basis of the Neph (cloud) analysis of the Tiros 3 data, a 400-n.mi. stretch from the California west coast toward Honolulu was forecast. This forecast, based on satellite cloud photographs proved to be very accurate. Figure 17 is presented to illustrate the extent of the stratus overcast that was present during the time of the NRL flight. It is a single satellite photograph [21] obtained from a television camera and covers the last 600 n.mi. along the route to San Diego. The Tiros television camera uses a linear scanning system of 500 raster lines per frame, which at a 500-n.mi. height above earth would give a 1 to 3 n.mi. width to each. Consequently, small clouds less than the raster line spacing would not be detectable on the photograph.

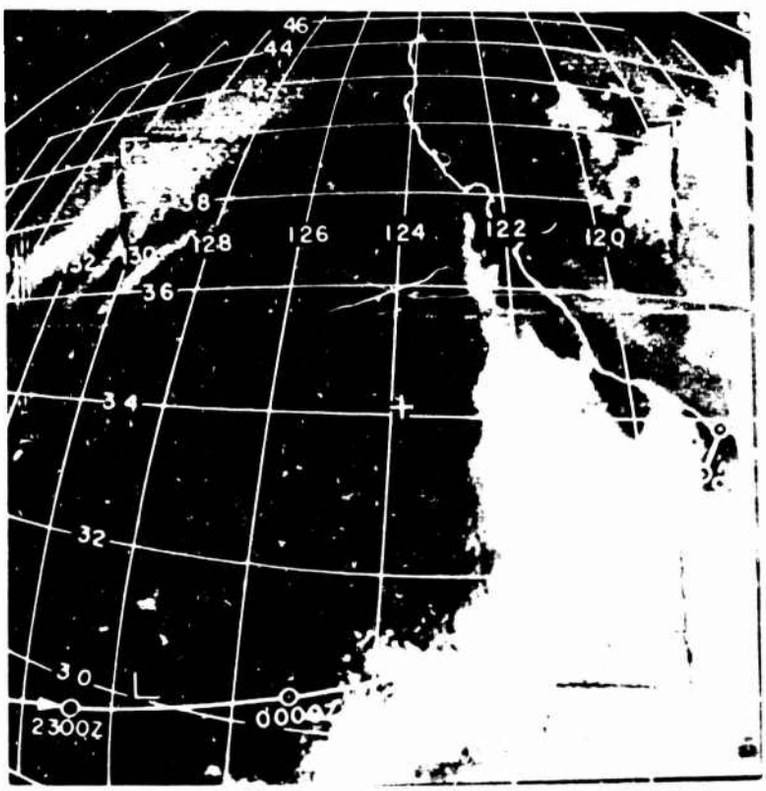

Fig. 17 — Overcast conditions near southern California, Tiros 3, 638-8, Aug 25, 1961, 2123 05Z [21]

A cloud mosiac showing the areas covered by clouds on both sides of the aircraft track for over one-half the route is presented in Fig. 18. The cloud mosaic is made from a compilation of individual satellite cloud photographs. Hourly positions of the aircraft are shown for the last 7 hr of flight. A confident prediction of a continuous elevated duct for any of the continuous stratus overcast areas shown in the cloud mosaic from the California coast to approximately 125° W longitude can be made on the basis of previously observed radar signal measurements over this route. The use of similar satellite cloud photographs is a definite aid in predicting large-scale propagation conditions.

THE STATE OF THE ART IN MAKING A REFRACTIVE INDEX FORECAST

The ability to make an accurate real-time RIF for specific oceanic regions on a global basis is of special concern to naval operations. At best this service is very limited or nonexistent. To make reliable forecasts it is necessary to have a network of observing stations that can measure refractive indexes accurately. It is also essential to have a stockpile of climatological records that would give local geographic summaries of what is statistically expected in terms of refractive index profiles. Having such information would give fleet commanders and other naval operational personnel a better background knowledge of what to expect in strategic areas on a monthly or seasonal basis. Present-day global synoptic meteorological and oceanographic forecasting services are enhanced by the utilization of computerized forecasting techniques. Short-range forecasts (less than a day) and long-range surface and upper-air forecasts of 5 days or more are routinely supplied for almost any geographic region in the world. Where atmospheric forecasts are needed, the prime source of measuring the significant meteorological parameters of pressure, temperature, and humidity for the past generation comes from an international global network of weather stations that makes use of atmospheric profiles obtained from ascending balloonborne radiosonde measurements.

The radiosonde is a slow-response instrument that measures temperature, pressure, and moisture content of the air while being carried aloft by a lighter-than-air balloon, which eventually bursts, often above 100,000 ft. Most computer forecasts using radiosonde data make use of smoothing, or averaging, techniques that do not require fast-response-time instruments to get desired forecast results. A RIF, however, requires both accurate and fast-response measuring instruments, especially for the vapor pressure and temperature parameters. Consequently, the use of radiosonde data seriously limits the ability to detect accurately the significant refractive index gradients needed to obtain a reliable RIF. Currently, the best instrument for obtaining an atmospheric profile of refractive indexes is an airborne microwave refractometer, which has been used only sparsely since the 1950's, mainly by research and reconnaissance type aircraft.

RECOMMENDATIONS

Action should be initiated to establish a central depositor for the collection and filing, in a computerized system, of all refractive index profile measurements obtained by microwave refractometers and to require all commands to forward routinely all such data to the designated record center within a reasonable time. In this manner a stockpile of reference material would be available eventually for statistical summary and use by those

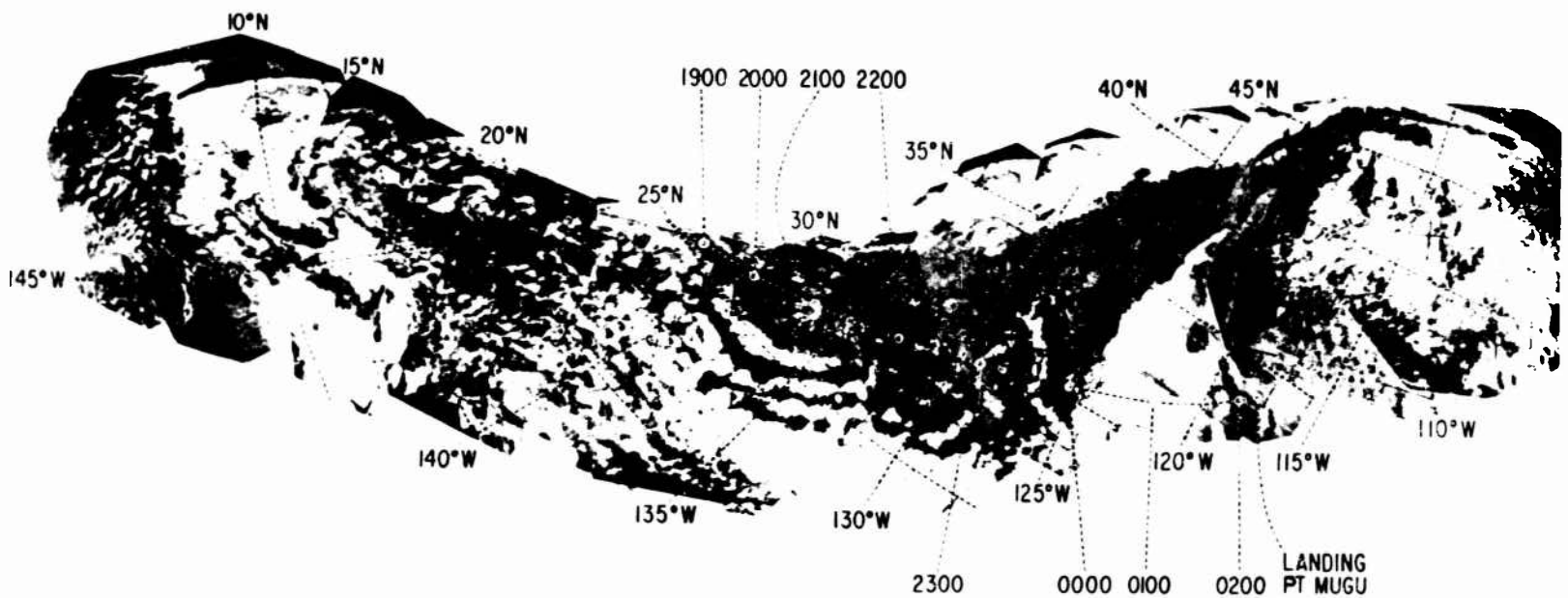

Fig. 18—Cloud mosaic of photographs from Tiros 3, August 25, 1961 [21]

having a need for such data. In this respect, it would also be advisable for the Navy, where possible, to collect all known past microwave refractometer records because the cost to resurrect and use this type of data would be nominal when compared to the cost of obtaining similar records by performing new flights in the areas where the data were first observed.

A computerized ray-tracing capability should be developed by means of which a ship commander could obtain the best available forecast in the area of concern by making use of on-the-spot data to generate a two-dimensional computerized family of ray paths that would best describe the presence of anomalous propagation conditions.

Other methods should be developed, such as satellite cloud photography, that would allow cloud correlation techniques to give a secondary forecast capability on a global real-time basis from existing forecast centers via Teletype or satellite communication links.

More atmospheric model cases should be developed that could possibly be used in conjunction with satellite cloud coverage photography, large-scale synoptic weather patterns, weather reconnaissance data, or any other significant weather relationship that can be correlated to give a RIF.

A reference atlas of ray-tracing profiles should be compiled that could be used to characterize, or correlate, typical past weather conditions with present synoptic weather.

A committee of naval civilian and military scientists experienced in the field of electromagnetic wave propagation should be established to review and update the present knowledge of anomalous propagation so that this information can be more advantageously used to improve the state of the art of making a RIF.

New research programs that would enhance the state of the art of making a RIF, should be initiated.

REFERENCES

1. H.G. Booker, "Some Problems in Radio Meteorology," *Quart. J. Roy. Meteorol. Soc.* 74, 277-307 (1948).
2. D.R. Jones, "Meteorological Refractive Effects Upon Radar Wave Propagation," NAVAER 50-1 P-527, July 1, 1954, p. 8; prepared at Project AROWA, U.S. Fleet Weather Control, Norfolk, Va.
3. D.E. Kerr, editor, *Propagation of Short Radio Waves*, Dover Publications, Inc., New York, 1965, p. 21.
4. M.I. Skolnik, *Introduction to Radar Systems*, McGraw-Hill, New York, 1962, p. 8.
5. W.F. Freiberger, editor, *International Dictionary of Applied Mathematics*, Van Nostrand, Princeton, N.J., 1960, pp. 851-852.
6. E.K. Smith, Jr., and S. Weintraub, "The Constants in the Equation for Atmospheric Refractive Index at Radio Frequencies," *Proc. IRE 41*, No. 8, 1035-1037 (Aug. 1953).

7. F.A. Berry, Jr., E. Bollay, and N.R. Beers, editors, *Handbook of Meteorology*, McGraw-Hill, New York, 1945, p. 373.

8. L.B. Battan, *Radar Meteorology*, 2d impression, The University of Chicago Press, Chicago, 1960, p. 18.

9. *CRC Standard Mathematical Tables*, 10th ed., Chemical Rubber Publishing Co., Cleveland, 1954, p. 15.

10. NWRF 31-0660-035, "Meteorological Aspects of Radio-Radar Propagation," U.S. Navy Weather Research Facility, Norfolk, Va., 1960, pp. 46-69.

11. B.R. Bean, B.A. Cahoon, C.A. Sampson, and G.D. Thayer, *A World Atlas of Atmospheric Radio Refractivity*, U.S. Department of Commerce Environmental Science Services Administration, U.S. Government Printing Office, Washington, D.C., 1966.

12. H.L. Crutcher and O.M. Davis, "U.S. Navy Marine Climatic Atlas of the World," Volume VIII in *The World*, NAVAIR 50-1C-54, Mar. 1, 1969.

13. C.G. Purves, "Synopsis of December 1960 Flight of Project Tradewinds IV," NRL Ltr. Rept. 5270-32, NRL Problem R07-05, Aug. 23, 1961.

14. C.G. Purves, "Synopsis of February 1961 Flight of Project Tradewinds IV," NRL Ltr. Rept. 5270-34, NRL Problem R07-05, Aug. 23, 1961.

15. Wave Propagation Branch Rept. "220-Mc Propagation in an Elevated Duct," Report of NRL Progress, Washignton, D.C., May 1960, pp. 1-15.

16. H. Ficker, Veröff. Meteor. Inst. Berlin I, No. 4 (1936).

17. H. Riehl, *Tropical Meteorology*, McGraw-Hill, New York, 1954, pp 63, 65-66.

18. C.G. Purves, "Meteorological Aspects of Radio Propagation in Tradewind Areas," in *Proceedings of the Fifth Navy Science Symposium*, ONR-9, Vol. 3, pp. 812-822, Office of Naval Research, Washington, D.C., 1961.

19. N.W. Guinard, M.B. Laing, and K. Morin, "Ray Tracing in Rising and Falling Ducts," NRL Rept. 6253, June 22, 1965.

20. P.L. Shereschewsky and P. Wehrle, "Les Systems Nuageau," *Off. Nat. Meteor. Memo.* No. 1, Paris, 1923.

21. C.G. Purves, "A Month-by-Month Study of the Elevated Duct Between San Diego and Hawaii," NRL Memorandum Report 1416, Apr. 3, 1963.